Biochemistry

pubs.acs.org/biochemistry
Article

Revisiting the Roles of Catalytic Residues in Human Ornithine Transcarbamylase

Samantha S. Watson, Emily Micheloni, Lisa Ngu, Kelly K. Barnsley, Lee Makowski, Penny J. Beuning,* and Mary Jo Ondrechen*

Cite This: *Biochemistry* 2024, 63, 1858−1875

ABSTRACT: Human ornithine transcarbamylase (hOTC) is a mitochondrial transferase protein involved in the urea cycle and is crucial for the conversion of toxic ammonia to urea. Structural analysis coupled with kinetic studies of *Escherichia coli*, rat, bovine, and other transferase proteins has identified residues that play key roles in substrate recognition and conformational changes but has not provided direct evidence for all of the active residues involved in OTC function. Here, computational methods were used to predict the likely active residues of hOTC; the function of these residues was then probed with site-directed mutagenesis and biochemical characterization. This process identified previously reported active residues, as well as distal residues that contribute to activity. Mutation of active site residue D263 resulted in a substantial loss of activity without a decrease in protein stability, suggesting a key catalytic role for this residue. Mutation of predicted second-layer residues H302, K307, and E310 resulted in significant decreases in enzymatic activity relative to that of wild-type (WT) hOTC with respect to L-ornithine. The mutation of fourth-layer residue H107 to produce the hOTC H107N variant resulted in a 66-fold decrease in catalytic efficiency relative to that of WT hOTC with respect to carbamoyl phosphate and a substantial loss of thermal stability. Further investigation identified H107 and to a lesser extent E98Q as key residues involved in maintaining the hOTC quaternary structure. This work biochemically demonstrates the importance of D263 in hOTC catalytic activity and shows that residues remote from the active site also play key roles in activity.

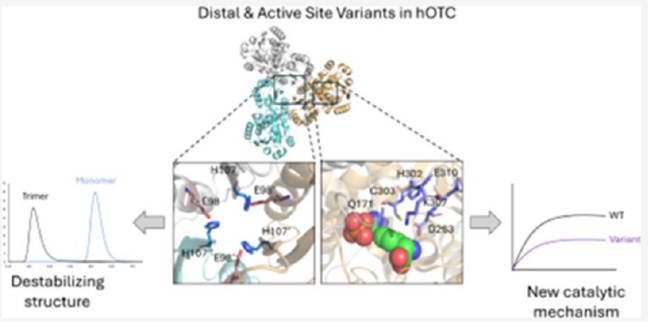

INTRODUCTION

Human ornithine transcarbamylase (hOTC) is a mitochondrial transferase protein expressed in the liver and is essential for safely removing neurotoxic ammonia from the body as urea. The biochemical function of hOTC is to synthesize L-citrulline (CIT) from L-ornithine (ORN) and carbamoyl phosphate (CP), releasing inorganic phosphate (Figure 1).[1] The citrulline product is ultimately converted into arginine, from which the guanidino group is removed as urea. Mutations to the OTC gene result in OTC deficiency (OTCD), which is the most common inherited urea cycle disorder, affecting one in 14 000−77 000 individuals.[2−4]

OTC is active as a homotrimer with each subunit consisting of 322 amino acids and a molecular weight of 36 kDa (Figure 2). Active sites located near each of the three subunit interfaces comprise the CP and ORN binding domains. Residues in two subdomains that belong to different regions of the amino acid sequence interact with CP and ORN. Residues 90−94 are identified as binding to the phosphate group of CP, while residues 168−171 are identified as being involved in the binding of the carbamoyl group, based on the crystal structure and conserved domains in *Escherichia coli* and rat OTC and *E. coli* aspartate transcarbamylase (ATCase).[5−7] Both motifs 90−94 and 168−171 are conserved across the transferase family, emphasizing the importance of these residues for catalytic function; these residues are colored yellow in Figure 2.[6,8] The ORN binding domain, colored green in Figure 2, consists of residues 263−267 and 302−305, with residues 263−267 including the flexible SMG loop that is critical for binding ORN.[9,10] C303, located in the subdomain involving residues 302−305, has been hypothesized to be an essential active site residue.[9,11] A sequence alignment and a structural alignment of a diverse set of OTC proteins can be found in Figures S1 and S2, respectively.

Most of the current information about OTCD has been obtained through clinical and genomic studies.[7,12] Additionally, crystal structures of hOTC with the bisubstrate analogue *N*-

Received: April 18, 2024
Revised: June 3, 2024
Accepted: June 18, 2024
Published: June 28, 2024

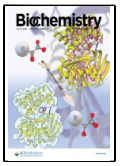

https://doi.org/10.1021/acs.biochem.4c00206
Biochemistry 2024, 63, 1858−1875

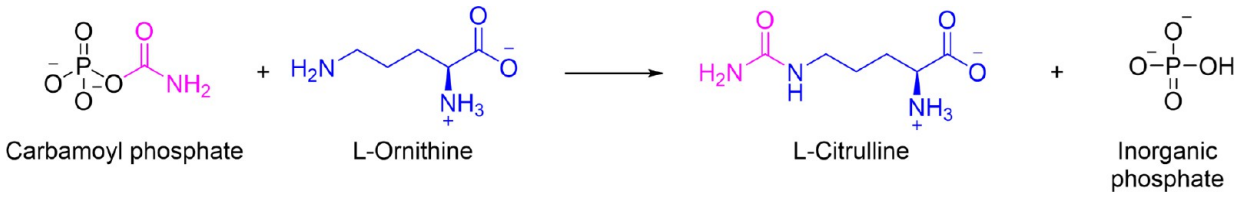

Figure 1. Reaction catalyzed by OTC. The side chain amino group from L-ornithine (blue) performs a nucleophilic attack on the carbonyl carbon atom of carbamoyl phosphate (pink). Charge rearrangement releases the phosphate and forms L-citrulline. L-Ornithine is shown as deprotonated on the basis of current understanding of OTC's catalytic mechanism.[27]

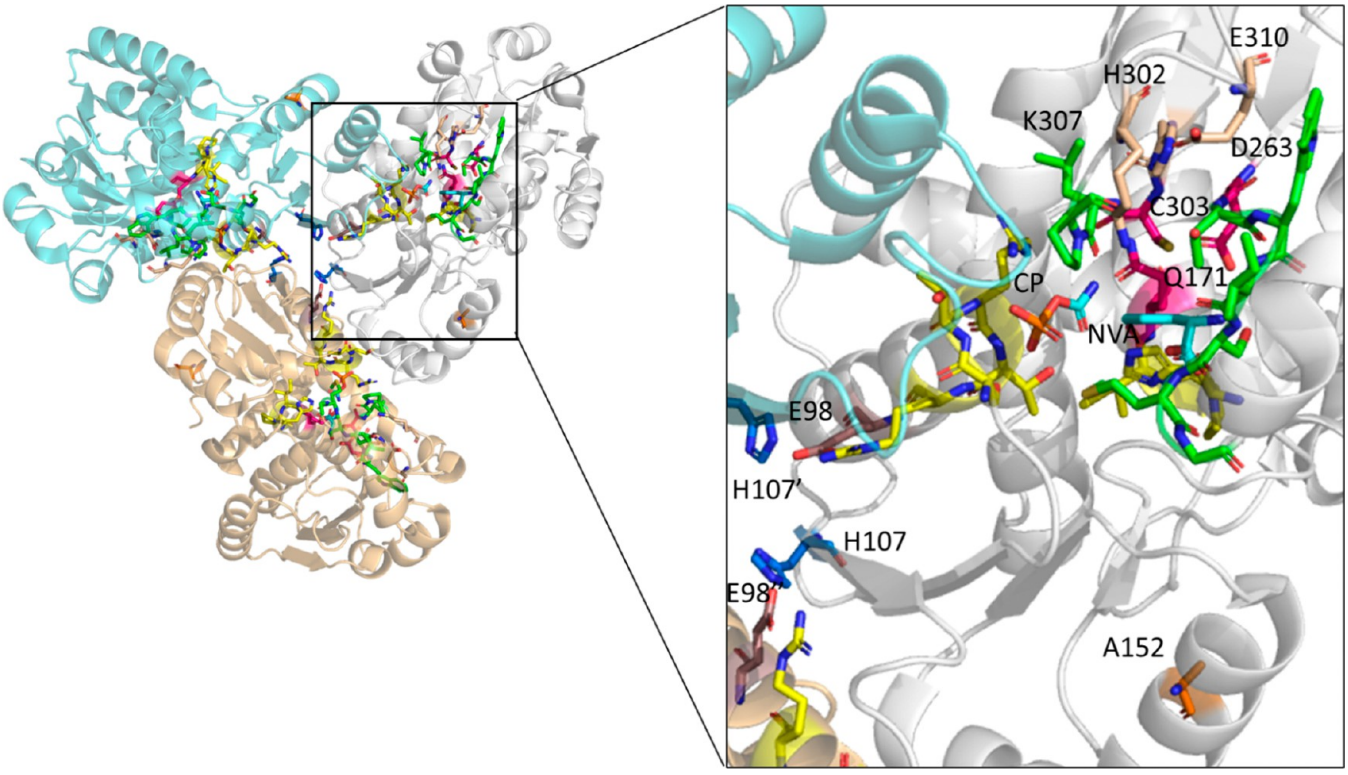

Figure 2. Crystal structure of hOTC1C9Y[9] displaying the quaternary structure, active site residues, and residues tested. Each monomer subunit is highlighted in a different color. NVA and CP, colored by atom with nitrogen in blue, oxygen in red, phosphate in orange, and carbon in cyan, highlight the residues tested here and their distance from the active site. ORN binding residues 263−267 and 302−305 are colored green. CP binding residues 90−94 and 168−171 are colored yellow. First-shell residues Q171, D263, and C303 are colored pink. Second-shell residues H302, K307, and E310 are colored tan. Third-shell residue E98 and fourth-shell residue H107 are colored brown and dark blue, respectively. Finally, fifth-shell residue A152 is colored orange. Prime and double-prime designations indicate blue and tan subunits, respectively.

phosphonoacetyl-L-ornithine (PALO),[5] CP,[9] and CP with L-norvaline (NVA), an ornithine analogue,[13] have allowed comparison to conserved substrate binding motifs observed within the transferase family. Structural analysis coupled with kinetic studies of *E. coli*, rat, bovine, and other transferase proteins has shed light on residues that play key roles in substrate recognition and conformational changes[5,13,14] but has not provided direct evidence for the active residues involved in mammalian OTC function. This study identifies amino acid residues of hOTC that participate in its biochemical function and proposes an updated mechanism of catalysis for hOTC.

The experimental work reported herein is guided by computational tools developed by us to identify active residues, including distal residues involved in biochemical activity. Partial Order Optimum Likelihood (POOL) is a machine learning method that rank-orders all amino acids in an input protein three-dimensional structure by the probability of catalytic importance.[15,16] Metrics obtained from the theoretical titration curves from THEMATICS (theoretical microscopic anomalous titration curve shapes)[17,18] and ligand binding pocket information from ConCavity[19] are the input features utilized by POOL to generate the amino acid ranking. Catalytic residues are partially protonated over a larger pH range, compared to residues that are not biochemically active, and therefore exhibit a perturbed computed titration curve.[17,20] POOL has been shown to be highly successful in identifying catalytically active residues, including distal residues,[21−26] and was used to prioritize amino acids to test experimentally. The top-ranked set of residues from POOL for hOTC consists of known or previously predicted catalytic residues along with distal residues not previously linked to catalytic activity. In this work, we determine the catalytic importance of residues likely to be involved in hOTC function and report analysis of the roles of distal residues predicted by POOL that make up a multilayer active site.

https://doi.org/10.1021/acs.biochem.4c00206
Biochemistry 2024, 63, 1858−1875

MATERIALS AND METHODS

POOL Predictions of Active Residues. The monomer of hOTC [Protein Data Bank (PDB) entry 1OTH, chain A; UniProt entry P00480[10]] was preprocessed in YASARA[28] to add missing atoms, followed by energy minimization. POOL utilizes the theoretical titration curves of ionizable residues from THEMATICS[17] to generate environmental variables to incorporate all 20 amino acid types, together with surface topology information from the structure-only version of ConCavity,[19] to rank-order all residues according to their probability of involvement in biochemical activity, including catalytic and ligand binding residues in an enzyme. The preprocessed PDB file for hOTC was used as the sole input. The THEMATICS metrics used as input features were those described previously.[16] The output files provide a ranked list of all amino acids in the protein ordered according to the probability of involvement in catalysis or ligand recognition. The top-ranked residues from POOL were annotated to identify known catalytic residues, disease-related residues, and, importantly, residues not previously identified in either category. All residue scores were normalized to the highest POOL score, and residues with values of >0.01 were predicted to contribute to biochemical activity.[24]

Electrostatic Coupling Analysis. Poisson−Boltzmann calculations were performed as previously described[16] on PDB entry 1OTH;[10] a bound ornithine molecule was included in the calculation. Coulomb interaction energies, intrinsic pK_as, and pK_a values were computed as previously described.[20,29]

Site-Directed Mutagenesis. Unless otherwise noted, all materials and reagents were purchased from Fisher or Research Products International. A pET21a plasmid expressing human OTC was a gift from Dashuang Shi (Children's National Medical Center). Variants were prepared with a Quikchange site-directed mutagenesis kit (Agilent) using mutagenic DNA primers (Eurofins Operon Biotechnologies) and verified by DNA sequencing (Eton Bioscience, Charlestown, MA).[13,30]

Protein Expression and Purification. Wild-type (WT) hOTC and its variants were expressed in BL21 (DE3) Tuner cells with pGro7 encoding chaperone proteins (Takara) and grown on Luria broth (LB) agar plates supplemented with 100 μg/mL ampicillin and 25 μg/mL chloramphenicol. The plates were incubated overnight (16−20 h) at 37 °C. A single colony was isolated and grown in 20 mL of LB at 37 °C overnight. The overnight culture was used to inoculate 1 L of LB supplemented with 100 μg/mL ampicillin, 25 μg/mL chloramphenicol, and 2.5 g/L arabinose, which was used to induce expression of the chaperone proteins. Once the culture reached an OD_{600} of 0.6−0.8, the expression of hOTC protein was induced with 100 μM isopropyl β-D-1-thiogalactopyranoside (IPTG), and the mixture cooled to room temperature (~20−23 °C) and shaken for 16−20 h. Once growth was complete, the cells were collected by centrifugation at 6000g for 10 min and stored at −80 °C until purification.

The hOTC protein contains a His tag and involves a one-step, 10 mL nickel column purification to isolate the WT hOTC protein and its variants. The pellet was prepared by thawing overnight at 4 °C in 30 mL of His A buffer [50 mM HEPES, 500 mM NaCl, 5 mM imidazole, and 10% glycerol (pH 7.4)], 100 μM phenylmethanesulfonyl fluoride (PMSF), and half a protease inhibitor cocktail tablet (Roche). The thawed pellet was then sonicated for a total of 5 min at 10 s intervals, lysed by adding lysozyme, and mixed for 30 min on a shaker at 4 °C. The lysed cells were then centrifuged at 16000g for 1 h to collect the supernatant, which was then filtered using a 0.45 μm filter and loaded onto the nickel column (two 5 mL Cytiva HisTrap HP columns). The column was washed with His A buffer and protein was eluted at 300 mM imidazole with a His B buffer [50 mM HEPES, 500 mM NaCl, 500 mM imidazole, and 10% glycerol (pH 7.4)] gradient. Fractions were analyzed by 12% sodium dodecyl sulfate−polyacrylamide gel electrophoresis to identify those containing the pure protein of interest. These fractions were pooled and dialyzed against storage buffer [50 mM HEPES, 200 mM NaCl, 2 mM EDTA, and 10% glycerol (pH 7.4)] for 4 h. The pooled protein was then collected and concentrated using Vivaspin 5−10 kDa concentrators. The concentration was determined by a Bradford assay, and proteins were aliquoted and stored at −80 °C for several months without a loss of activity.

Kinetic Assay. The activity of hOTC was determined using the colorimetric determination of the product citrulline using diacetyl monoxime (Sigma).[31] A discontinuous assay was performed in 96-well plates with 100 μL of enzyme reaction mixture collected and quenched at a given time point. The blank consisted of 100 μL of reaction mixture before the enzyme was added to the well and 500 μL of color reagent. Reactions were initiated with 20 μL of the hOTC enzyme at final concentrations of 10−800 nM and varying substrate concentrations. For the experiment, 100 μL of the reaction mixture was collected at time points from 0.25 to 10 min, and the reaction quenched in the corresponding color reagent. The chromogenic reagent consists of 100 mL of a diacetyl monoxime solution (5 g of 2,3-butanedione monoxime and 1 L of distilled water), 200 mL of an acid ferric solution (200 mL of concentrated phosphoric acid, 250 mL of concentrated sulfuric acid, 250 mg of ferric chloride, and 550 mL of distilled water), and 10 mg of thiosemicarbazide (TSC).[32] Due to the volatility of these reagents, the color reagent was used within 1 h of preparation. The standard curve was prepared by making a serial dilution of citrulline dissolved in protein storage buffer ranging from 0.00033 to 0.167 mM in the reactions with 500 μL of color reagent. Then, the plate was sealed, heated in a 100 °C water bath for 5 min, and then rapidly cooled in a 15 °C cold bath for 20 min, which allowed color development.[23] After the plates had been incubated and cooled, 200 μL from each well was transferred to a clear 96-well plate for the determination of OD_{530} with a Biotek Synergy HT Plate Reader and Gen5 version 1.11.

The blank OD value for each corresponding condition was subtracted from each time point of the reaction OD value. A standard curve was used to calculate the amount of citrulline produced in each well. The initial velocity for each substrate condition was determined and fit to the Michaelis−Menten equation using GraphPad Prism 5.02 for Windows (GraphPad Software, La Jolla, CA) to determine K_m and V_{max} with respect to ORN and CP, respectively, for WT hOTC and its variants. The reported values represent the average and standard deviation from at least three experiments.

Thermal Shift Assay. The melting temperatures of WT hOTC and its variants were determined with a Bio-Rad c1000 Touch Thermal Cycler (CFX96 Real Time System) and Bio-Rad CFX Manager version 3.1.1517.0823. The reaction mixtures were assembled in 96-well PCR plates with a final volume of 20 μL per well by mixing 4 μM enzyme in storage buffer, sterile filtered water, and 2 μL of 100× Sypro Orange to achieve a final concentration of 10×. Substrates were added to

https://doi.org/10.1021/acs.biochem.4c00206
Biochemistry 2024, 63, 1858−1875

obtain final concentrations of 30 mM ORN, 100 mM CP, 10 mM L-norvaline (NVA), 10 mM sodium phosphate, and 10 mM Cit. The blank consisted of Sypro Orange dye and water for apo conditions and the corresponding substrate when applicable. The temperature was increased from 4 to 100 °C in 0.2 °C increments and held at each temperature for 10 s.[23,33] The melting temperature was obtained for WT hOTC and each variant by identifying the peak minima of the first derivative plot of the relative fluorescence (RFU) versus temperature (T). The reported values represent the average and standard deviation from at least three experiments.

Microscale Thermophoresis. Monolith NT.Automated (Nanotemper) was used to determine the dissociation constants of the variants for CP. Each variant was diluted with 50 mM HEPES, 150 mM NaCl, 0.05% Tween, and 2 mM EDTA to a concentration of 500 nM. A serial dilution of CP was performed in 384-well polystyrene nonbinding plates, and the 500 nM protein stock solution was added to each well for a final concentration of 250 nM in each well. The mixture was incubated at room temperature for at least 5 min before it was loaded onto a Monolith NT.Automated label free capillary chip (MO-AZ005) for the detection of the intrinsic tryptophan fluorescence. All variants were analyzed with a 10 s on time, and low, medium, and high MST ramps were used depending on the variant. The reported K_d and standard deviation were obtained from at least three trials.

Small Angle X-ray Solution Scattering (SAXS), Wide Angle X-ray Scattering (WAXS), and Size Exclusion Chromatography SAXS (SEC-SAXS). SAXS and in-line SEC-SAXS data were collected for WT hOTC and its variants with and without substrates at beamline I7A HP BioSAXS at the Cornell High Energy Synchrotron Source (CHESS), using a Superdex 200 5/150 GL column when applicable.[34,35] Additional SAXS and WAXS data were collected at beamline 16-ID LiX Life Science X-ray Scattering at Brookhaven National Laboratory National Synchrotron Light Source II (NSLII). At both beamlines, WT hOTC and its variants at 2.5−13 mg/mL with and without substrates were transported frozen in dry ice and gently thawed on ice on the day of data collection. For SEC-SAXS, solution scattering data were captured every 2 s for 2000 frames for the duration of the SEC run. Data were collected from the maxima of peak(s) representing the protein of interest, avoiding aggregates. Data for the running buffer were collected as a blank and then subtracted from the protein data to remove any scattering that was the result of the buffer. Unlike SEC-SAXS, which does not need a separate blank, SAXS/WAXS data collection consisted of measurements for the protein alone and with CP, buffer alone, and buffer with CP. This allowed for a blank for the protein and a blank for the protein with substrate CP. SAXS and WAXS data were collected every 1 s for 10 frames in a flow cell.

The analysis for SEC-SAXS consisted of plotting all 2000 frames in the RAW software.[36] The blank for the run was identified as an equilibrated portion of the chromatograph with a baseline reading before the protein eluted. The blank was then subtracted from the maximum peak where the protein eluted from the column. The subtraction of the blank from the protein scattering peak was plotted separately from the entire chromatography scan. The subtracted curve was then expressed as a Guinier plot to extract the radius of gyration (R_g), D_{max}, and $p(r)$ and a Kratky plot to visualize protein flexibility and stability. The Kratky plot was used to identify folded states of the protein and to ensure that the differences in R_g were due to structural changes in the presence of substrates and mutations made and not denaturation of the protein. A MATLAB (MathWorks, Natick, MA) locally weighted linear regression was used to smooth the data for the Kratky and semilog plots.

For the analysis of SAXS and WAXS data, the 10 scans collected for protein at each varying substrate condition and blank were plotted in RAW and merged into a single scan. The blanks were subtracted from their respective protein conditions in a manner similar to that of the SEC-SAXS analysis represented as Guinier and Kratky plots. The ATSAS suite [version 2.8.4 (https://www.embl-hamburg.de/biosaxs/download.html)] was used to further process the SAXS data.[37,38] GNOM was used to normalize distance distribution plots $p(r)$, and GASBOR was used to generate *ab initio* models. Figures of protein envelopes were visualized using CHIMERA.[39]

GNOM and GASBOR within the ATSAS suite were used to determine the three-dimensional molecular envelopes of WT hOTC and its variants in the apo and ligand-bound forms using the solution X-ray scattering data.[37,38,40] GNOM was used to regularize and evaluate the pair distribution function of the SAXS data by using an indirect Fourier transform. GASBOR uses an ensemble of dummy residues (beads) and simulated annealing to build a "chain-compatible" structure that fits inside the maximum sphere calculated by the distribution plot for low q (SAXS) and high q (WAXS) values. Dummy atoms act as place holders for real atoms and occupy a known position in space. The number of dummy residues is approximately equal to the total number of amino acids in the hOTC construct (1062 residues). The GASBOR reciprocal space was used to fit the intensity of the distribution plot and, in general, yields a better fit to the experimental data.

To assess the uniqueness of these reconstructions, 10 bead models were generated with and without 3-fold symmetry. The final χ^2 values of these models ranged from 0.99 to 1.5. Each model was aligned with a trimeric crystal structure of hOTC (PDB entry 1OTH[10]) using SUPCOMB. The 10 aligned models were averaged to provide a three-dimensional reconstruction of the shape of hOTC with a partial specific volume set to the expected value from the hOTC molecular weight. The results were then visualized using Chimera.[39]

Determination of the Molecular Size by Size Exclusion Chromatography (SEC). The molecular weights of purified WT OTC and its variants were determined using SEC with a 26 mL Superdex 200 Increase (Cytiva) column at a rate of 0.250 mL/min. An isocratic elution of storage buffer [50 mM HEPES, 200 mM NaCl, 2 mM EDTA, and 2% glycerol (pH 7.4)] was used. Gel filtration standards (Bio-Rad catalog no. 1511901) were analyzed in the same buffer to develop a calibration curve, which was used to determine the molecular weight of the protein. The Bio-Rad standard vitamin B_{12} was omitted from the calibration curve because its molecular weight is 1.3 kDa, which is below the column's 10 kDa cutoff. WT hOTC and the E98Q and H107N variants were normalized by loading 50 μL of 2.0 mg/mL protein onto the column. For the analyses with CP, each variant was incubated with 10 mM CP on ice for 5 min before being loaded onto the column.

https://doi.org/10.1021/acs.biochem.4c00206
Biochemistry 2024, 63, 1858−1875

Table 1. Top POOL-Ranked Residues, and Other hOTC Residues Studied in This Work, with Their POOL Rankings and Distances from the Substrates Color-Coded on the Basis of the Distances in Figure 2[e]

Rank	Residue	Layer	Distance from Substrate (Å)	*E. coli* Alignment[c]	Disease Associated Mutations[d]	Normalized POOL score
1	CYS 303	1st	4.2[b]	1AKM: C273	C303G, C303R-Neonatal C303Y-Female	1.000
2	ASP 263	1st	2.7[b]	1AKM: D231	D263N, D263G-Female	0.638
3	GLU 326*	2nd	6.5[a]	1AKM: Near N318	E326K-Female	0.535
4	ASP 175*	3rd	9.4[b]	1AKM: D140	D175G-Late D175V-Female	0.301
5	HIS 302*	2nd	7.5[a]	1AKM: H272	H302R, H302Y-Neonatal H302A, H302L-Female H302Q-Late	0.265
6	GLU 98*	3rd	11.5[a]	1AKM: E63	E98K-Female	0.203
7	HIS 107*	4th	15.4[a]	1AKM: R72	no disease association	0.193
8	CYS 109*	4th	17.5[a]	1AKM T74	C109R-Female	0.171
9	ARG 330	1st	3.0[a]	1AKM: R319	R330G-Female	0.099
10	GLU 310*	2nd	8.1[b]	1AKM: E299	E310G, E310M-Late	0.055
11	ARG 94*	2nd	5.6[a]	1AKM:R59	R94T-Late	0.053
12	LYS 307*	2nd	6.4[b]	1AKM: Near V232	no disease association	0.029
13	ARG 141	1st	2.7[a]	1AKM: R106	R141G, R141P-Female R141Q-Female, neonatal	0.028
14	ARG 92	1st	3.2[a]	1AKM: R57	R92G-Female R92Q, R92L, R92P-Neonatal	0.016
15	HIS 168	1st	3.3[a]	1AKM: H133	H168P, H168Q-Late H168R-Female	0.011
37	GLN 171	1st	2.7[a]	1AKM: Q136	no disease association	0.002
314	ALA 152(-)	5th	20.5[a]	1AKM: A117	A152V-Late	0.000

[a]Distance from CP. [b]Distance from ORN. [c]*E. coli* OTC information from ref 23. [d]Information about disease-associated mutations from ref 7. [e]The rows highlighted in blue represent POOL-predicted residues that are not associated with disease. *Distal residues predicted by POOL.

RESULTS

POOL predicted 15 catalytically important residues for hOTC with a normalized POOL score above the 0.01 cutoff (Table 1).[23,24] The residues selected for this study were predicted to be (1) active site residues from the crystal structure but lacked biochemical characterization, (2) distal residues predicted by POOL that have no association with disease (Table 1), or (3) POOL-predicted residues at positions with disease-associated mutations that lack prior characterization. Distal residues are defined as residues that are not in direct contact with the substrate. First-layer residues are within 5 Å of a substrate and are generally in direct contact with it. Second-layer residues are not in contact with the substrate but are within 5 Å or in direct contact with first-layer residues. Third-layer residues are within 5 Å or in direct contact with second-layer residues, etc.

Four of the hOTC residues characterized here (Q171, D263, H302, and C303) have been previously identified from crystal structure analysis as likely to be important for binding ORN or CP but have not been biochemically analyzed.[5,10] Substrate binding residues H302 and Q171 were ranked fifth and 37th, respectively. POOL predicted two distal residues to play an important role in hOTC catalysis, fourth-layer H107 and second-layer K307, ranked seventh and 12th, respectively (Table 1). Third-layer residue E98, ranked sixth, was chosen to characterize its interactions with H107. Fifth-layer residue A152 was selected as a negative control, as it has a high sequence conservation score as determined by ConSurf[41] and a low POOL score with a POOL rank of 314. The distances of the residues with respect to the ligands can be found in Figure S3.

Using the POOL rankings as a guide, we constructed the following hOTC variants to evaluate their effect on activity: E98Q, H107N, A152V, Q171A, D263A, D263N, H302L, C303A, K307A, K307E, and E310Q. The POOL results ranked C303 and D263 as first and second, respectively, in terms of likelihood that they play important roles in substrate binding and/or catalytic activity. The D263A mutation was made to explore the loss of charge and polarity in the active site. The D263N mutation is an isosteric substitution and was made to assess the effects of removing a charge while maintaining polarity to determine how that might relate to the clinical manifestation of OTCD in patients.[42,43] The C303A mutation was made to compare the activity reported for rat and *E. coli* OTC to that of hOTC, noting that C303S and a cyano-derivatized C303 have been shown to impact ORN substrate binding.[13,14,44,45] For His, mutations to Asn and Leu were made to maintain the size. For H302L, in the ORN binding site, polarity was removed to examine the effects on the CP−ORN tetrahedral transition state. The Q171A mutation, also in the ORN binding site, was made to examine the importance of a first-shell residue that is conserved in the transferase family as reported by the ConSurf server[41] but not known to have a disease-associated mutation. For distal residue K307 predicted by POOL, mutations K307A and K307E were made in the second layer to determine the importance of the positive charge for the OTC activity. The H107N mutation in the fourth layer was made to maintain the polarity and size in the trimer core while testing the role of the proton transfer

https://doi.org/10.1021/acs.biochem.4c00206
Biochemistry 2024, 63, 1858−1875

Table 2. Results of Steady State Kinetic Assays for hOTC WT and Its Variants with Respect to ORN

variant	layer	K_m (mM)	V_{max} (mM/min)	k_{cat} (s^{-1})	k_{cat}/K_m (M^{-1} s^{-1})	fold decrease in k_{cat}/K_m
WT		0.48 ± 0.12	0.021 ± 0.0052	34 ± 9.4	$(7.5 \pm 2.4) \times 10^4$	N/A
E98Q	third	0.28 ± 0.058	0.018 ± 0.00081	15 ± 1.9	$5.4 \times 10^4 \pm 4.3 \times 10^3$	1.4
H107N	fourth	0.34 ± 0.099	0.0065 ± 0.00044	5.7 ± 0.92	$1.6 \times 10^4 \pm 1.3 \times 10^3$	4.7
A152V[a]	fifth	0.33 ± 0.055	0.027 ± 0.0016	23 ± 1.3	$(7.2 \pm 1.8) \times 10^4$	1.0
Q171A	first	1.1 ± 0.0077	0.0032 ± 0.00041	2.6 ± 0.34	$2.3 \times 10^3 \pm 3.2 \times 10^2$	32
D263A[b]	first	–	–	–	–	–
D263N	first	170 ± 29	0.0042 ± 0.00055	0.088 ± 0.011	$(0.52 \pm 9.5) \times 10^{-2}$	1.4×10^5
H302L	second	8.0 ± 1.9	0.024 ± 0.0018	10 ± 1.8	$1.3 \times 10^3 \pm 1.4 \times 10^2$	58
C303A	first	6.3 ± 0.050	0.011 ± 0.0014	19 ± 2.3	$3.0 \times 10^3 \pm 3.4 \times 10^2$	25
K307A	second	8.0 ± 1.5	0.0029 ± 0.00018	5.2 ±. 88	$6.1 \times 10^2 \pm 52$	120
K307E	second	1.5 ± 0.26	0.0023 ± 0.00022	2.0 ± 0.18	$1.4 \times 10^3 \pm 4.0 \times 10^2$	54
E310Q	second	2.2 ± 0.35	0.012 ± 0.0035	10 ± 2.9	$4.5 \times 10^3 \pm 6.0 \times 10^2$	17

[a]Negative control. [b]For D263A due to the solubility limit of ORN and low activity, saturation was not reached at pH 7.4 or 8.0 and no activity was detected.

Table 3. Results of Steady State Kinetic Assays for hOTC WT and Its Variants with Respect to CP

variant	layer	K_m (mM)	V_{max} (mM/min)	k_{cat} (s^{-1})	k_{cat}/K_m (M^{-1} s^{-1})	fold decrease in k_{cat}/K_m
WT		0.21 ± 0.053	0.017 ± 0.0046	29 ± 7.6	$1.4 \times 10^5 \pm 4.5 \times 10^4$	N/A
E98Q	third	0.27 ± 0.049	0.018 ± 0.00061	15 ± 1.7	$5.5 \times 10^4 \pm 8.2 \times 10^3$	2.5
H107N	fourth	2.4 ± 0.56	0.0061 ± 0.00043	5.1 ± 0.52	$2.1 \times 10^3 \pm 7.7 \times 10^2$	66
A152V[a]	fifth	0.29 ± 0.023	0.026 ± 0.0019	22 ± 1.5	$7.5 \times 10^4 \pm 5.0 \times 10^3$	1.9
Q171A	first	1.7 ± 0.34	0.0035 ± 0.00029	2.9 ± 0.25	$1.8 \times 10^3 \pm 2.8 \times 10^2$	79
D263A[b]	first	–	–	–	–	–
D263N	first	0.54 ± 0.18	0.012 ± 0.0020	0.25 ± 0.038	$4.8 \times 10^2 \pm 8.5 \times 10$	3.0×10^2
H302L	second	5.6 ± 0.99	0.023 ± 0.0019	9.5 ± 1.2	$1.8 \times 10^3 \pm 2.4 \times 10^2$	78
C303A	first	0.21 ± 0.061	0.0090 ± 0.0012	15 ± 2.0	$(7.3 \pm 1.2) \times 10^4$	2.0
K307A	second	0.035 ± 0.0074	0.033 ± 0.00015	5.6 ± 0.39	$1.7 \times 10^5 \pm 5.8 \times 10^4$	0.87
K307E	second	0.036 ± 0.0057	0.0019 ± 0.00030	1.6 ± 0.25	$4.6 \times 10^4 \pm 8.9 \times 10^3$	3.1
E310Q	second	0.31 ± 0.063	0.010 ± 0.0021	8.5 ± 1.8	$(3.0 \pm 1.1) \times 10^4$	4.8

[a]Negative control. [b]For D263A due to the solubility limit of ORN and low activity, saturation was not reached at pH 7.4 or 8.0 and no activity was detected.

capability. Once we determined that H107N impacts the quaternary structure of the hOTC and we noted the proximity of E98 across the subunit interface and the high POOL score of E98, we created E98Q, a third-layer variant, to test how the removal of charge from this residue near H107 affects the trimer structure. The E310Q mutation maintains size and polarity while probing the role of the negative charge of glutamic acid in the active site. The A152V mutation was made as a control, as it has a high sequence conservation score as determined by ConSurf[41] and a low POOL score with a POOL rank of 314, and was predicted to have a minimal effect on protein function.

Electrostatic Coupling Analysis. Electrostatic potential calculations on the hOTC structure with ornithine bound identified the residues most strongly coupled to ORN and to the active site residues, together with their intrinsic pK_as.[20,29] (The intrinsic pK_a of an amino acid is the pK_a in the hypothetical protein structure, where all other ionizable groups are in their charge-neutral state.) The side chain of ORN is strongly electrostatically coupled to three arginines, R92, R141, and R330, with Coulomb coupling energies of 1.1, 2.5, and 1.3 kcal/mol, respectively (Table S1). The strong Coulombic coupling to the three positively charged residues reduces the effective pK_a of the conjugate acid of the amine side chain of ORN to an estimated 6.5, helping to make its deprotonated state available to act as a nucleophile. The residues most strongly coupled to residue D263 include POOL-predicted residues H302, C303, and E310 and the side chain of the bound ORN (Table S2).

Mutations of POOL-Predicted Residues Impact Catalysis and Stability. Steady state kinetic assays (Figures S4 and S5) were carried out for WT hOTC and its variants with respect to ORN and CP (Tables 2 and 3, respectively). The hOTC C303A variant exhibited a 25-fold decrease in catalytic efficiency with respect to ORN and a minimal change in activity with respect to CP, similar to observations from previous work with rat and *E. coli* OTC.[13,14,23,44] Although the hOTC variant C303A shows a significant loss of activity, it was not as large as that observed with the hOTC D263A and D263N variants. The hOTC D263N variant showed a 140 000-fold decrease in catalytic efficiency with respect to ORN and a 300-fold decrease with respect to CP; the hOTC D263A variant had no detectable activity. Variants E98Q, H107N, Q171A, H302L, K307A, and K307E showed 1.4−120-fold decreases in catalytic efficiency with respect to ORN. Variants E98Q, H107N, Q171A, H302L, K307A, and K307E showed 0.87−79-fold decreases in catalytic efficiency with respect to CP. In addition to hOTC D263 variants, hOTC Q171A and H302L were the other variants that exhibited substantial decreases in catalytic activity with respect to both substrates. Mutation of fourth-layer residue H107 in the hOTC H107N variant, which is nearly 20 Å from CP, resulted in a 66-fold decrease in catalytic efficiency compared to WT hOTC, with respect to CP, although it had less than a 5-fold decrease

https://doi.org/10.1021/acs.biochem.4c00206
Biochemistry 2024, 63, 1858−1875

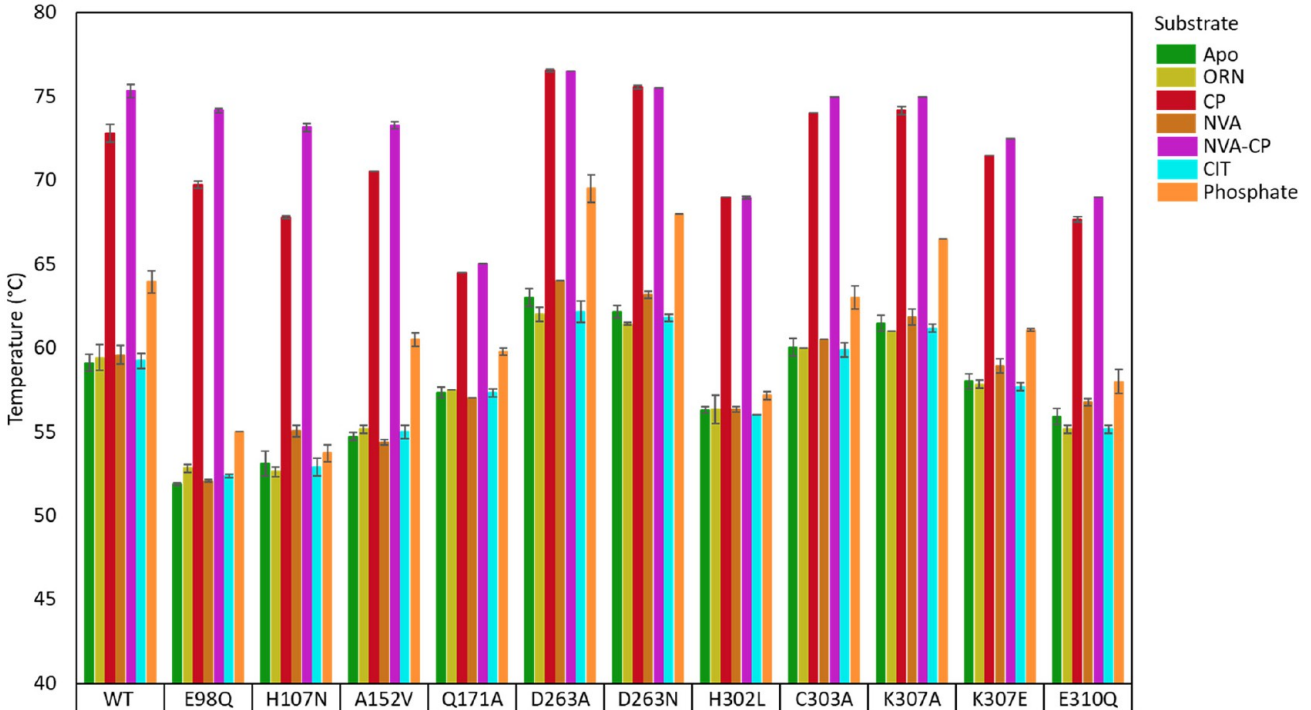

	WT	E98Q	H107N	A152V	Q171A	D263A	D263N	H302L	C303A	K307A	K307E	E310Q
Apo	59	52	53	55	57	63	62	56	60	61	58	56
ORN	59	53	53	55	58	62	61	56	60	61	58	55
CP	73	70	68	71	65	77	76	69	74	74	72	68
NVA	60	52	55	54	57	64	63	56	61	62	59	57
NVA-CP	75	74	73	73	65	77	76	69	75	75	73	69
CIT	59	52	53	55	57	62	62	56	60	61	58	55
Phosphate	64	55	54	61	60	70	68	57	63	67	61	58

Figure 3. Melting temperature (T_m) of WT hOTC and its variants. T_m values are indicated below the graph.

in activity with respect to ORN. As expected, hOTC A152V had catalytic efficiencies similar to those of WT hOTC.

To determine the effects of the mutations on protein stability, thermal shift assays were performed with WT and the 11 hOTC variants with and without a substrate. Seven conditions were tested: apo, with ORN, with CP, with Cit, with phosphate, with NVA, and with NVA with CP. This allowed a comparison of the stability of WT hOTC and its variants with and without substrates (Figure 3).

The thermal shift assay with apo hOTC variants showed a T_m change within ±4 °C of the T_m for WT hOTC (59 ± 0.5 °C), indicating that the stabilities of most of the variants were similar to that of WT OTC, except for hOTC H107N and E98Q. The apo hOTC H107N and E98Q variants had melting temperatures of 53 ± 0.7 and 52 ± 0.1 °C, respectively. The addition of ORN did not substantially change the T_m for WT hOTC or any variant, which is expected because CP must bind before a conformational shift occurs allowing ORN to bind.[5] The most dramatic shift in melting temperature was with the addition of CP. In general, the variants had an increase in T_m of 12−18 °C in the presence of CP compared with those of their apo conditions. The hOTC Q171A variant had a T_m change of only 7 °C with the addition of CP, suggesting that the addition of CP does not stabilize this variant to the same degree as for the others.

Determining the T_m in the presence of both substrates ORN and CP would lead to product formation, which would complicate the analysis, so the ORN analogue NVA was used to probe the CP-induced increase in T_m for WT hOTC and its variants. NVA is smaller than ORN and lacks the amine group, but structures of ternary complexes of OTC with NVA and CP indicate that the combination of NVA and CP induces OTC to adopt a catalytically active conformation.[9,46] NVA alone did not substantially increase the melting temperature of WT hOTC or any of its variants. However, when NVA was added with CP, WT hOTC and its variants showed increases in T_m values of 8−22 °C. WT hOTC in the presence of NVA and CP has a melting temperature of 75 °C, which is 2 °C higher than that with CP alone. The variants with the largest changes in melting temperature in the presence of NVA-CP were hOTC E98Q, H107N, and A152V, which had increases of 22, 20, and 18 °C, respectively, from those under the apo conditions and 4, 5, and 2 °C increases, respectively, relative to those with CP alone. The other hOTC variants did not show an appreciable change in the presence of CP versus CP with NVA, indicating that the increase in stability is mostly due to CP.

To gain insight into how the products of the reaction affect the variants, melting temperatures were determined in the presence of citrulline and phosphate. The presence of citrulline did not change the melting temperature for any of the variants; all of the variants had a melting temperature within 1 °C of those under the apo conditions. The T_m of WT hOTC increased by 5 °C in the presence of phosphate. The T_m values of hOTC variants A152V, D263A, D263N, and K307A were increased between 5 and 7 °C in the presence of phosphate. However, the other hOTC variants showed smaller changes in

https://doi.org/10.1021/acs.biochem.4c00206
Biochemistry 2024, 63, 1858−1875

T_m between 1 and 3 °C in the presence of phosphate relative to their respective apo T_m values.

For most conditions, hOTC variants E98Q and H107N were markedly less stable than WT hOTC, although they still exhibited the characteristic large increases in T_m in the presence of CP and NVA with CP. hOTC variant Q171A showed modestly decreased T_m values across most conditions and had only relatively small increases in T_m in the presence of CP, phosphate, and NVA with CP, suggesting the decrease in catalytic activity of hOTC Q171A could be related to a decrease in level of stabilization in the presence of substrates. hOTC H302L showed an overall profile of T_m changes similar to that of hOTC Q171A, except that H302L showed an only slight increase in T_m in the presence of phosphate. Both hOTC Q171A and hOTC H302L variants show decreased activity with respect to both substrates, which could be due to the loss of stabilization by substrates resulting from a structural defect or decreased binding affinities of the substrates. On the contrary, the hOTC D263 variants show dramatic losses in activity but have T_m profiles similar to those of WT hOTC, suggesting that the D263A and D263N mutations do not impair the overall stability of hOTC.

The Binding of CP Is Affected by hOTC Mutation. To determine the effects of the different mutations on the binding of CP, dissociation constants (K_d) were determined for CP using microscale thermophoresis. WT OTC exhibited a K_d of 230 ± 110 nM for CP. hOTC variants C303A, D263A, and D263N all had K_d values similar to those of WT hOTC (Table 4). Therefore, the observed decrease in catalytic efficiency with respect to CP for hOTC variants D263A and D263N is not the result of a CP binding defect. hOTC variants H107N and H302L had weaker affinities for CP (Table 4). hOTC variants K307A, E98Q, E310Q, and A152V all showed moderate 5−12-fold increases in K_d (loss of affinity) compared to that of WT hOTC. Lastly, hOTC variants Q171A and K307E showed binding to CP; however, saturating conditions could not be met (Figure S6).

Table 4. Dissociation Constants (K_d) for the CP of hOTC Variants

variant	K_d, CP (nM)	fold increase in K_d (loss of affinity)
WT	$(2.3 \pm 1.1) \times 10^2$	N/A
E98Q	$(1.9 \pm 0.48) \times 10^3$	8.3
H107N	$(2.5 \pm 0.80) \times 10^4$	110
A152V	$(1.2 \pm 0.31) \times 10^3$	5.2
Q171A[a]	–	–
D263A	$(4.3 \pm 1.3) \times 10^2$	1.9
D263N	$(3.2 \pm 1.2) \times 10^2$	1.4
H302L	$(1.1 \pm 0.39) \times 10^5$	470
C303A	$(1.90 \pm 0.73) \times 10^2$	0.83
K307A	$(2.8 \pm 1.3) \times 10^3$	12
K307E[a]	–	–
E310Q	$(1.7 \pm 0.64) \times 10^3$	7.3

[a]Binding was detected; however, saturating conditions could not be obtained.

SEC-SAXS Reveals Conformational Change for Certain Variants. To probe the impact of these mutations on the hOTC conformation, SAXS scattering experiments were performed. SAXS does not require crystals and allows information about protein conformation in solution to be obtained. The hOTC variants were examined with and without CP, and the scattering curves were compared to those of WT hOTC. The WAXSIS[47] server was used to determine the R_g for the WT hOTC trimer to be 30.7 Å using the crystal structure (PDB entry 1OTH).[10] Analysis of the apo WT hOTC solution scattering curves shows soluble folded protein with a deviation of 4 Å from the predicted R_g value for the crystalline protein (Table 5). The variants have R_g values similar to that of WT hOTC (34.7 Å), except H107N, which has a smaller value of 28.6 Å, and hOTC H302L, which has a larger value of 39.5 Å. In addition, the presence of CP causes modest changes in R_g values of ≤1.0 Å, except for those of hOTC H107N and H302L, which showed increases in R_g in the presence of CP; these two variants, H107N and H302L, will be discussed in more detail below.

Table 5. Radii of Gyration (R_g) of WT OTC and Its Variants with and without CP from SEC-SAXS and SAXS

variant	layer	R_g, apo (Å)	R_g, CP (Å)
WT		34.7	34.5
H107N	fourth	28.6	31.3
A152V (−)	fifth	33.8	34.0
Q171A	first	33.9	34.2
D263A	first	35.8	35.7
D263N	first	34.9	34.8
H302L	second	39.5	41.2
C303A	first	34.9	34.6
K307E	second	34.3	33.9
K307A	second	35.0	34.0
E310Q	second	34.0	34.8

The Kratky plots for WT hOTC and its H107N and H302L variants show that all of the proteins are folded (Figure 4). The Kratky plots for WT hOTC and the H302L variant show two peaks, which usually indicates a multidomain protein. However, the Kratky plot for hOTC H107N shows only one peak. This observation together with an R_g value smaller than that of WT hOTC and the lower T_m value observed in the thermal shift assay as well as the location of the mutation at the trimer interface could indicate that the H107N variant has a perturbed quaternary structure relative to that of WT hOTC. The Kratky and semilog plots for the remaining variants can be found in Figure S7.

SAXS Envelopes for Selected Active Site Variants. Analysis of the crystal structures and ultraviolet difference spectra suggest that OTC undergoes a conformational change induced by the binding of CP.[5,9,48,49] Specifically, CP binds first and brings the domains into a more closed conformation; then ornithine binds, and the SMG loop moves over the active site. On the basis of comparisons of multiple crystal structures of both human and *E. coli* OTC, the binding of CP is thought to shift the angle between the domains by a few degrees even though the exact measurements are unknown because there is no crystal structure of apo human OTC.[5] The reconstructed envelopes for WT hOTC (Figure 5) show little change in the envelope of the protein in the presence of CP, which suggests that SAXS cannot resolve the small shifts in the domain or movement of the SMG loop. hOTC H107N has the smallest radius of gyration of all of the variants. Indeed, the reconstruction shows that the apo hOTC H107N variant is predominantly a dimer while hOTC H107N with the addition of CP is a trimer, indicating the presence of the substrate brings the subunits together (Figure 6). The SAXS data for

https://doi.org/10.1021/acs.biochem.4c00206
Biochemistry 2024, 63, 1858−1875

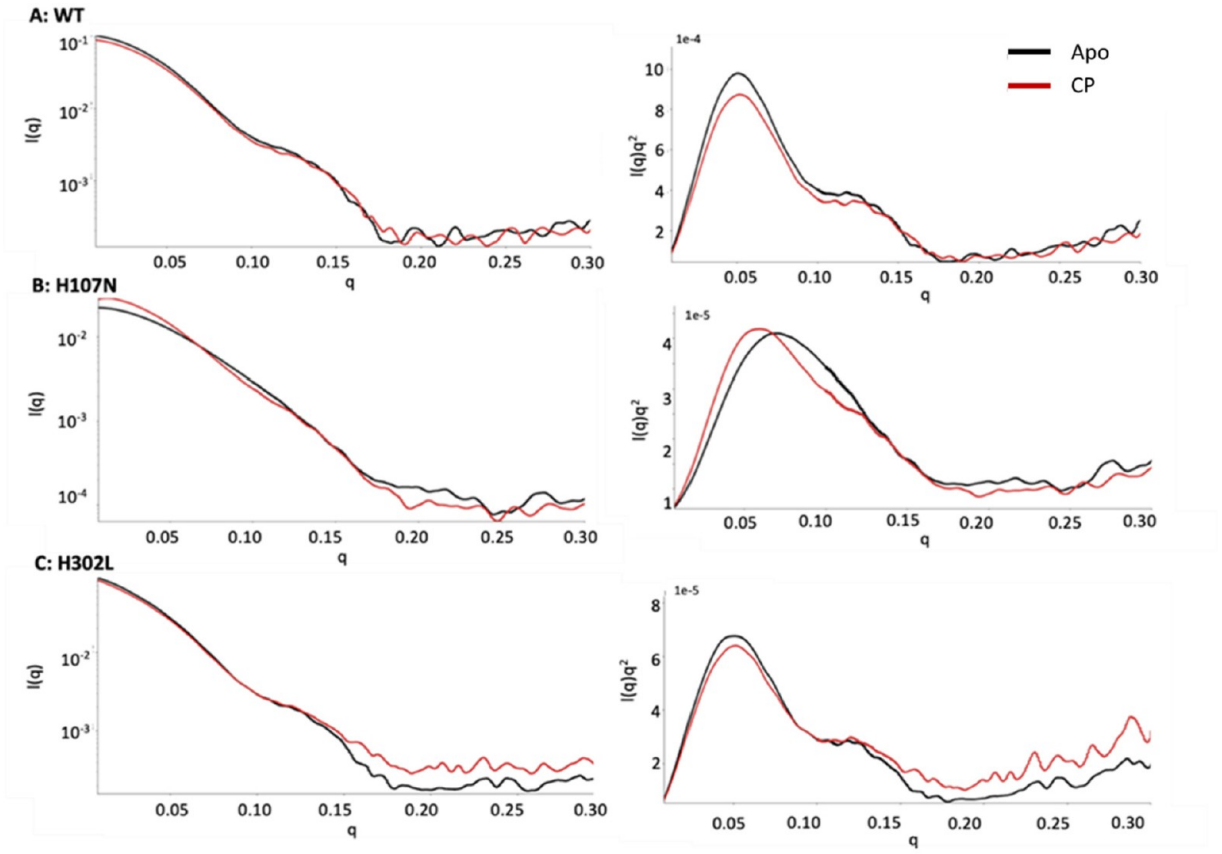

Figure 4. Semilog and Kratky plots for WT hOTC and variants H107N and H302L. (A) Analysis of the Kratky plot showed that the WT protein is folded. (B) The Kratky plot for hOTC variant H107N shows that the protein is folded and the plot lacks the two peaks expected for hOTC. (C) hOTC H302L is folded and the Kratky plot is similar to that of WT hOTC with no indication of a substantial change in protein flexibility. The curve for the apo condition is colored black; the curve for the enzyme with CP is colored red.

hOTC H107N in the absence of CP are consistent with a molecular weight of ∼54 kDa, which suggests the presence of both monomer and dimer forms of hOTC H107N. In the presence of CP, hOTC H107N has a molecular weight of 81 kDa, which corresponds to the dimeric and trimeric forms of hOTC H107N. Apo hOTC H302L also has an envelope similar to that of WT hOTC (Figure 7); however, the hOTC H302L R_g of 39.5 Å is larger than that of WT hOTC (Table 5). In the presence of CP, hOTC H302L has the largest R_g of 41.2 Å, indicating a less compact and less stable structure compared to that of WT, consistent with the fact that the H302L mutation is associated with disease.

Size Exclusion Chromatography. Due to the changes observed from SAXS analysis, especially the distributions of populations of hOTC H107N, we further probed the structures of hOTC H107N and hOTC E98Q using SEC. WT hOTC elutes at 12.7 mL and corresponds to the intact trimer, ∼107 kDa (Figure 8 and Figure S8). hOTC H107N showed a peak clearly shifted from that of WT hOTC (Figure 8). The majority peak eluted at 15.5 mL, which has a calculated molecular weight of 30 kDa. A second smaller and broader peak eluted at 13.6 mL, which could correspond to the dimer with a calculated molecular weight of 71 kDa (Figure 8). This suggests that the H107N mutation disrupts the trimer core of the protein and destabilizes the variant, shifting the equilibrium mainly to monomers. A series of increasing concentrations of hOTC H107N was applied to the SEC column (Figure S9); there was a modest shift in the elution volume, consistent with an increase in the molecular weight. hOTC variant E98Q shows similar results, except for a much broader distribution. The majority peak of hOTC E98Q elutes at 13.1 mL, which corresponds to a molecular weight of 90 kDa, most likely indicating the presence of the dimer and trimer. The E98Q variant also has a high degree of tailing in its elution profile, suggesting the presence of the dimer and monomer and showing that the mutation destabilizes the trimer core, although to a lesser extent than the H107N mutation. When the concentration of E98Q was increased, a shift in elution volume was not observed (Figure S10). The shoulder peak of E89Q eluted at ∼15.8 mL, which corresponds to ∼27 kDa. The molecular weight is much smaller than that of the monomer of OTC; therefore, we used HullRad[50] to calculate the theoretical hydrodynamic radius of the OTC monomer. The rotational hydrodynamic radius was calculated to be 27.3 Å, which could explain why the molecular weight that was observed by SEC was calculated to be <36 kDa, because SEC separates compounds on the basis of the hydrodynamic radius. These types of profiles were not observed with the other variants, which had elution profiles similar to that of WT with calculated molecular weights, suggesting they are intact as trimers (Figure S8).

To determine if the presence of a substrate would shift the equilibrium to higher-molecular weight species, WT hOTC and its E98Q and H107N variants were incubated with 10 mM CP before being loaded onto the column. However, in the presence of CP, the elution profiles of WT hOTC and its

https://doi.org/10.1021/acs.biochem.4c00206
Biochemistry 2024, 63, 1858−1875

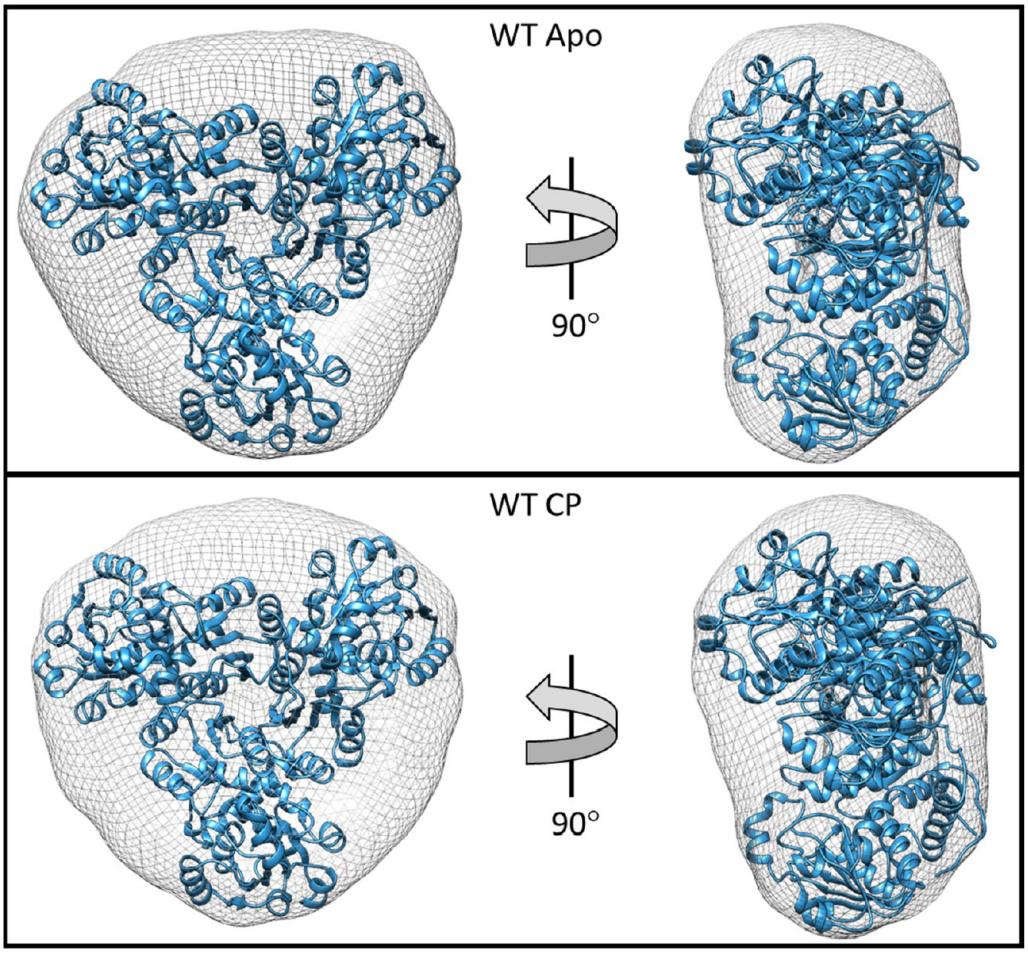

Figure 5. Reconstructed envelopes for apo WT hOTC and WT hOTC with CP.

E98Q and H107N variants remain essentially unchanged from those under their apo conditions (Figure 8).

DISCUSSION

Update to the Proposed Mechanism of the Reaction for hOTC: Involvement of C303 and D263. In this work, we used the active residue predictor POOL to predict the residues that are important for activity in hOTC. Substrate binding residues as well as residues more remote from the active site were predicted by POOL, and the predictions were tested by site-directed mutagenesis. We identified D263 as being critical for activity; it is noted that the aligned D231 in *E. coli* OTC also contributes significantly to catalysis[23] (*vide infra*). Residue D263 is in the SMG loop, and the D263-X264-X265-X266-S267-M268-G269 motif is a conserved aspartate/ORN binding site in aspartate transcarbamylase (ATCase) and *E. coli* OTC (Figure 9A).[5] This SMG loop has been shown to be flexible and to move into the active site once ORN binds.[5,10] A mutation in this loop could alter this motion, allowing the substrate to bind but creating an altered interaction with the loop. The kinetic results reported here highlight the importance of D263 for hOTC activity and suggest that it is the essential catalytic residue, playing a more important role in catalysis than C303. We previously observed a similar trend in *E. coli* OTC with the corresponding residues, in which mutation of D231 (corresponding to hOTC D263) had a far larger impact on enzymatic activity than mutation of C273 (corresponding to hOTC C303).[23] In a recent paper, 1570 hOTC variants were screened in a yeast Δ*arg3* mutant for their functional impact.[51] In general, the mutations of D263 led to more hindered growth than did those of C303. The D263V, D263A, D263Y, and D263H mutations led to the amorphic phenotype, which is below 5% WT OTC activity. Even D263N and D263E impaired growth. Mutations of C303 conferred amorphic phenotypes, but only when C303 was mutated to aromatic residues. hOTC variant C303G conferred moderate growth, consistent with a low but detectable activity level in human cell culture experiments,[52] whereas hOTC variant C303S was characterized as unimpaired in the yeast experiment.[51]

On the basis of an analysis of the crystal structures of hOTC complexed with PALO and CP-NVA (PDB entries 1OTH[10] and 1C9Y,[9] respectively) and *Mycobacterium tuberculosis* (*Mtb*) OTC (PDB entry 2I6U[46]), two mechanisms have been proposed for OTC catalysis. One mechanism suggests C303 as the catalytic residue in the active site. According to that proposed mechanism, D263 interacts with C303, increasing the basicity of the C303 thiol side chain, which interacts with the ε-amino group of ORN to deprotonate and activate ORN.[9] The kinetic data and calculated Coulomb couplings reported here, along with previous work characterizing rat OTC C271, support the interaction of C303 with ORN and show a functional relationship, but this interaction alone does not imply that C303 is the catalytic residue.[13] Indeed, the crystal structure of *Mtb* OTC (PDB entry 2I6U) indicates that on the basis of the distance and angle between the C303 and D263

https://doi.org/10.1021/acs.biochem.4c00206
Biochemistry 2024, 63, 1858−1875

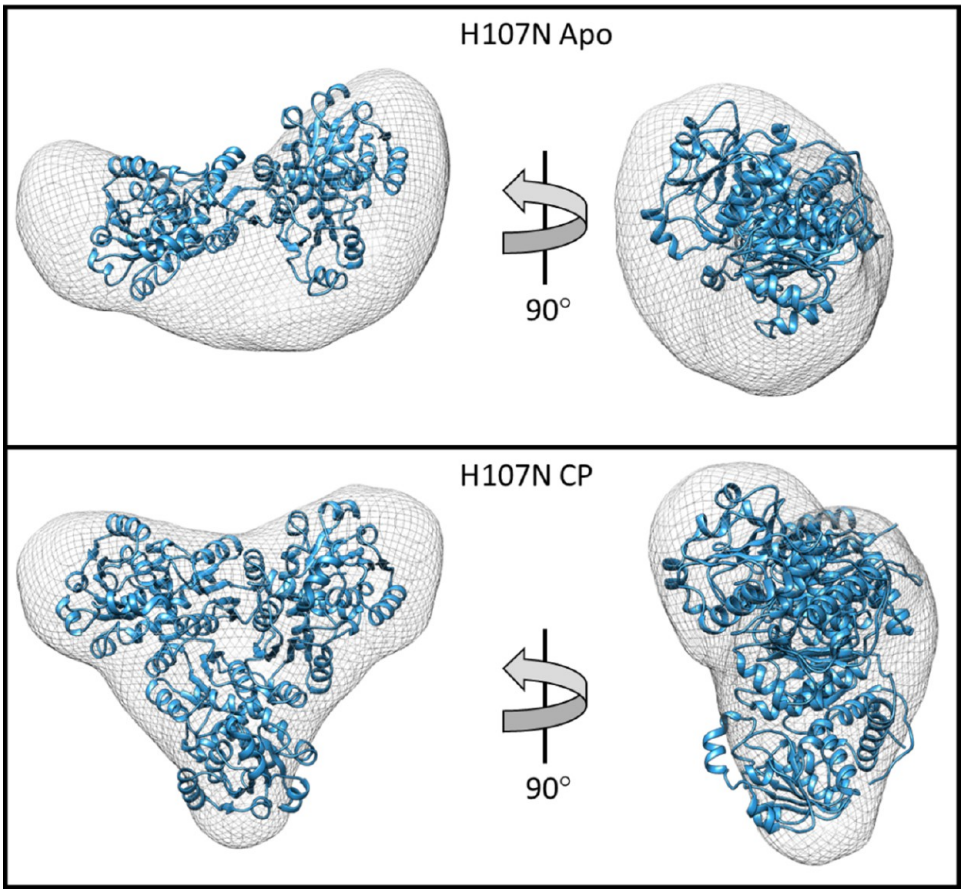

Figure 6. Reconstructed envelopes for apo hOTC H107N and hOTC H107N with CP.

side chains, once CP and ORN are bound, D263 cannot be an acceptor of the C303 S^{γ} hydrogen atom.[46] From this structure, a second mechanism is proposed in which ORN enters the active site of OTC with a side chain that is already deprotonated and therefore neutral, with a positively charged α-amino group. The hydrogen bonds between positively charged residues R52, R101, and R292 (R92, R141, and R330, respectively, in hOTC) and CP in addition to the polar interactions of D224 $O^{\delta 2}$, S228 O^{γ}, and N160 O^{δ} (D263 $O^{\delta 2}$, S267 O^{γ}, and N199 O^{δ}, respectively, in hOTC) with the α-amino group of NVA in the *Mtb* OTC structure would make the binding of ORN with a positively charged ϵN unlikely. This proposed mechanism does not explain how ORN, a nonproteinogenic amino acid that has a primary amine side chain, would be deprotonated in the pH 7.7−8.2 environment of the mitochondrial matrix.[53]

Our biochemical analysis suggests a variation of the first proposed catalytic mechanism for hOTC. As previously suggested from the structures of hOTC complexed with PALO and CP-NVA,[9,10] we suggest a protonated ORN enters the active site of hOTC. Indeed, in the mitochondrial milieu, the ORN side chain would be >99% protonated. The work presented here identifies D263 as the primary catalytic residue. When C303 is mutated to Ala, D263 can still serve as a catalytic base that, along with the electrostatic potential created by adjacent positively charged residues (*vide supra*), activates ORN for nucleophilic attack on CP. When D263 is mutated to Asn or Ala, substantial activity is lost. The kinetic results for the hOTC C303A variant highlight that C303 contributes to hOTC activity, but the C303A variant maintains substantial activity. In the context of hOTC C303A, $O^{\gamma 1}$ of D263 can promote a deprotonated side chain amino group of ORN but with less efficiency than in the context of WT hOTC, suggesting that C303's main role may be to help position ORN for reaction with the D263 side chain. Noting that C303 is the strongest Coulombic coupling partner of D263 (Table S2), we find that C303 may also help to activate D263.

Indeed, this theory seems to be supported by previous biochemical work. The C303S mutation in rat OTC increased the K_M 5-fold to 3.7 mM with respect to ORN, and its k_{cat} was reduced 20-fold with respect to ORN at pH 8.5.[13] Human OTC harboring the cyano derivative of C303 also performed similarly, only decreasing the catalytic efficiency with respect to ORN.[45] The kinetic values with respect to CP remained unchanged in both these variants, which is similar to our findings (Tables 1 and 2), where the efficiency with ORN is decreased but that with CP remains unchanged, indicating C303's role in positioning ORN for catalysis.

The polarity of the hypothetical protein structure with all ionizable groups in their electrically neutral states results in an intrinsic pK_a of 8.6 for the side chain of ORN, substantially lower than the value for free ornithine of just above 10. Strong Coulombic coupling to three arginine residues (R92, R141, and R330) in the active site region (Table S1) further decreases the pK_a value to ∼6.5. Reaction with D263 to deprotonate the side chain of ORN then enables ORN to serve as a strong nucleophile.

Biochemical Data Offer Support for Active Site and Remote Residues. hOTC Q171 is a first-shell residue in the H168-P169-I170-Q171 motif, which is conserved in the

https://doi.org/10.1021/acs.biochem.4c00206
Biochemistry 2024, 63, 1858−1875

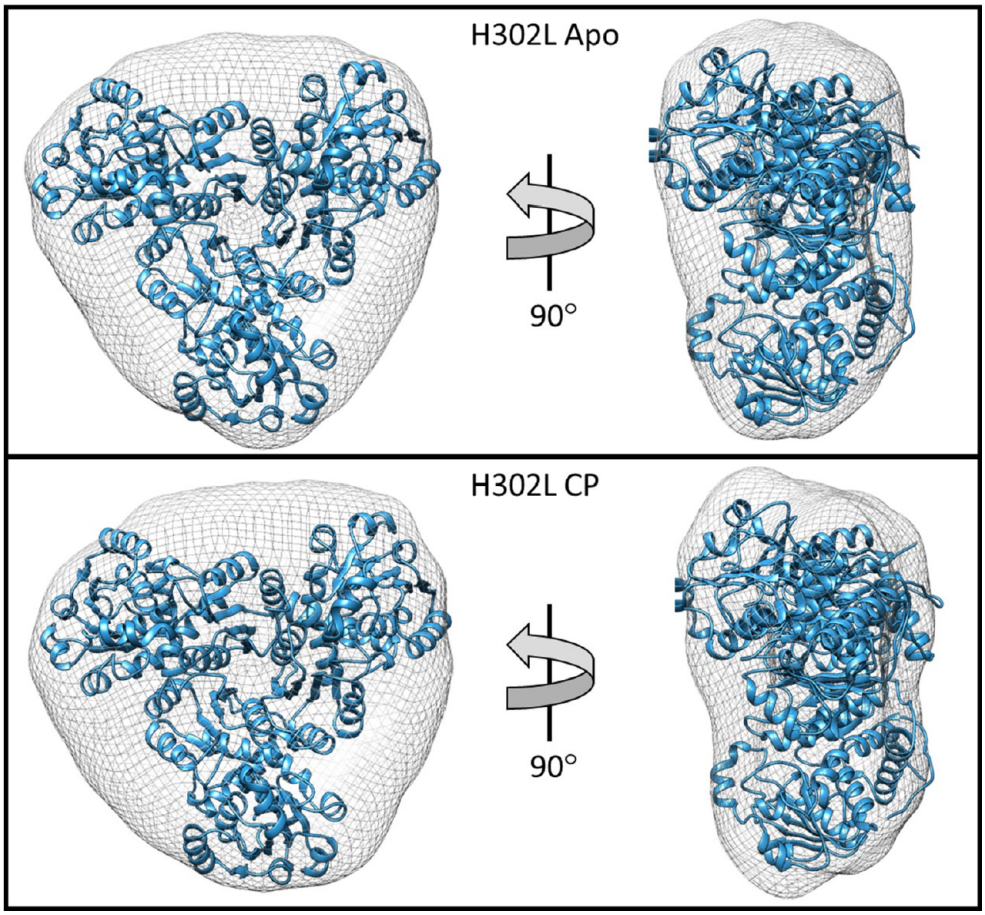

Figure 7. Reconstructed envelopes for apo hOTC H302L and hOTC H302L with CP.

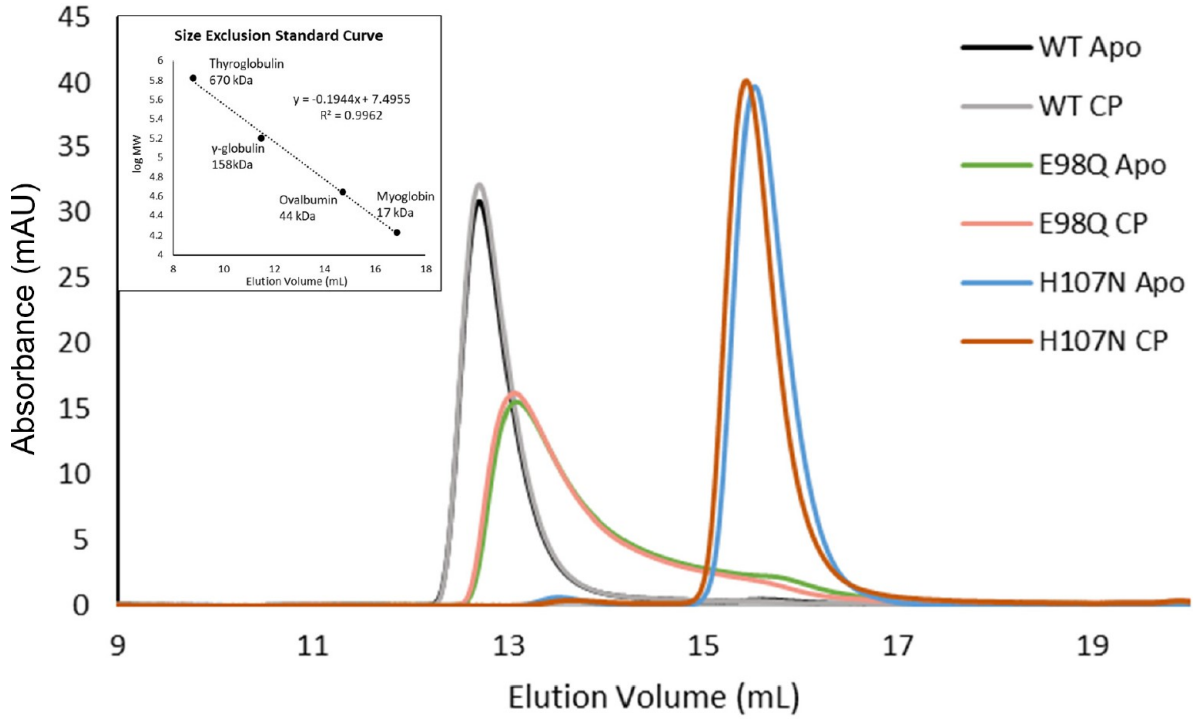

Figure 8. Size exclusion chromatogram comparing WT hOTC and its H107N and E98Q variants, illustrating the difference in the elution profiles and calculated molecular weights of the proteins.

https://doi.org/10.1021/acs.biochem.4c00206
Biochemistry 2024, 63, 1858−1875

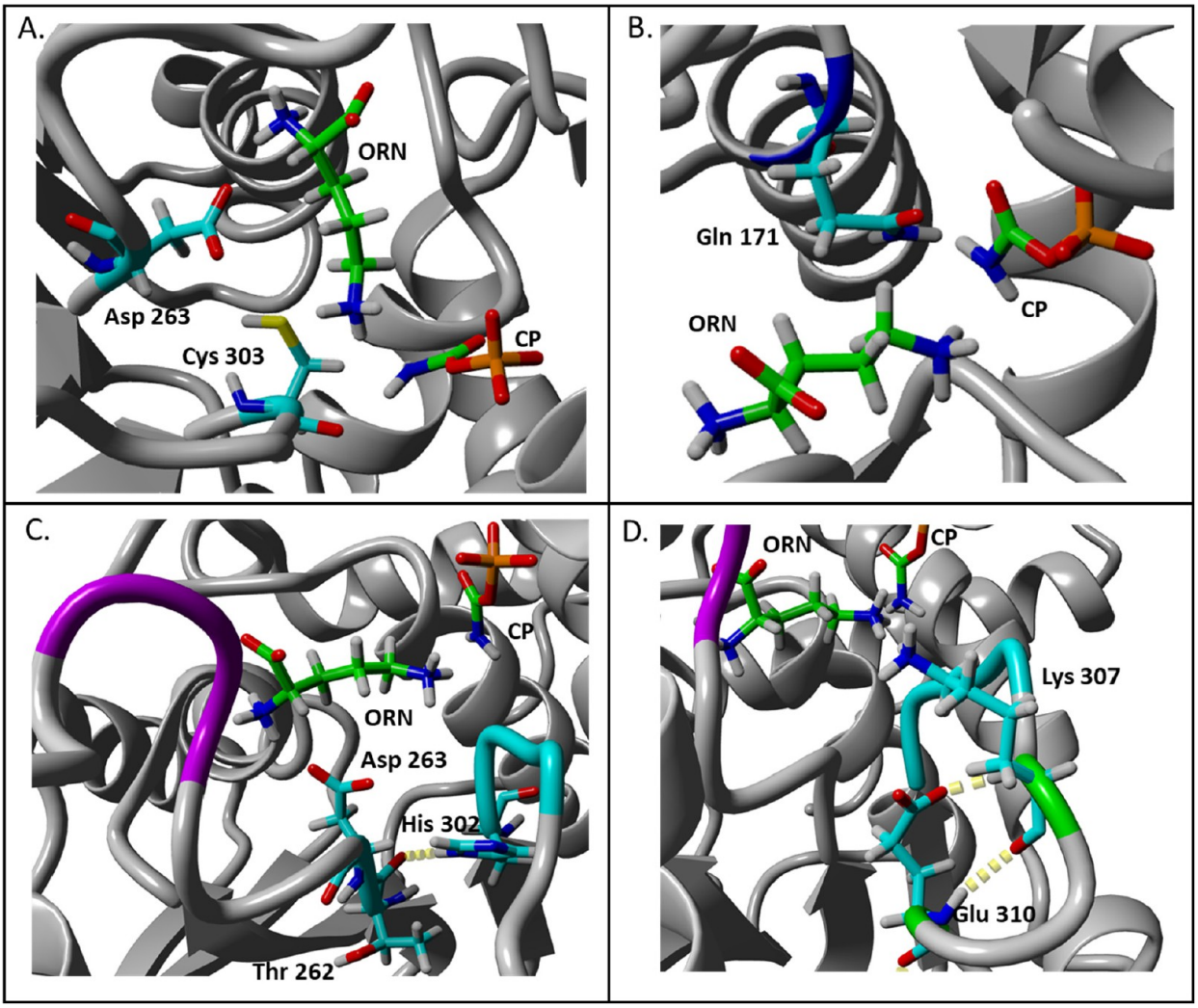

Figure 9. (A) Positions of D263 and C303 relative to each other and to the substrates ORN and CP. (B) Relative position of first-shell residue Q171 in the 168−171 motif implicated in binding of the carbamoyl group of CP. (C) Hydrogen bond between H302 and T262 shown by dotted yellow lines. The 302−305 loop is colored cyan, and the SMG loop purple. (D) Yellow dots show the K307 and E310 hydrogen bonds. The 302−305 loop is colored cyan, and the SMG loop purple.

transcarbamylase family as HPXQ, with ATCase experiments indicating that this loop contributes to the polarization of the carbamoyl group of CP (Figure 9B).[8,54] hOTC variant Q171A had a 32-fold decrease in catalytic efficiency with respect to ORN and a 79-fold decrease in catalytic efficiency with respect to CP. Upon removal of the polar side chain at Q171 in the hOTC Q171A variant, the carbamoyl group on CP is less stabilized and the electrophilicity of the carbamoyl carbon atom is reduced. In addition, hOTC Q171A showed the smallest increases in T_m in the presence of CP or NVA with CP of all of the variants, and a K_d for CP was not obtained because saturating conditions could not be achieved. This mutation clearly affects the enzyme's ability to bind CP, which could be the reason for its decreased catalytic efficiency. Indeed, hOTC Q171A also conferred a severe growth defect when expressed in a yeast arginine auxotroph when the polar residue was replaced with nonpolar and basic amino acids. The only mutation of Q171 that did not render the mutant amorphic was Q171E (Table 6).[51]

H302 is a second-shell residue that is involved in the conserved H302-C303-L304-P305 motif in hOTC, which is part of the ORN binding site (Figure 9C). Residue H302 is part of a motif believed to stabilize the CP−ORN tetrahedral intermediate.[9] Normally, when CP and ORN bind, H302 forms a hydrogen bond with T262, which is part of the SMG loop. The H302L mutation removes the hydrogen bond between H302 HN^{ε} and T262 O^{α}. This could alter the hydrogen bonding network of D263, affecting catalysis as shown by the decrease in activity with respect to ORN in the hOTC H302L variant. The decrease in the activity of hOTC H302L with respect to CP is most likely due to the loss of interactions between H302 and T262, which alters the D263 network. H302 is also strongly electrostatically coupled to D263, with a computed Coulomb energy of interaction of 1.9 kcal/mol (Table S2). The near match of the intrinsic pK_as (the pK_a inside the protein if all other sites were in their charge-neutral states), 3.5 for D263 and 3.7 for H302, fits the criterion[20] for buffer range expansion, an important property for catalytic residues.[17] Loss of this Coulombic coupling in the hOTC H302L variant thus weakens the catalysis. The importance of this residue is also highlighted as most of the mutations to H302 led to severely impaired growth and amorphic phenotypes in yeast.[51] Mutations H302L, H302D, H302P, and H302Y all showed <5% growth of WT, and

https://doi.org/10.1021/acs.biochem.4c00206
Biochemistry 2024, 63, 1858−1875

Table 6. Summary of Mutation Effects

mutation	activity	T_m[a]	K_d (CP)[b]	SEC	normalized growth in yeast[c]
WT		+++	+++	trimer	
E98Q	1.4-fold loss, ORN 2.5-fold loss, CP	lowest melting temperature	++	monomer, dimer, and trimer observed	hypomorphic
H107N	4.7-fold loss, ORN 66-fold loss, CP	++	110-fold	monomer and dimer observed	hypomorphic
A152V	1-fold loss, ORN 1.9-fold loss, CP	+++	+++	trimer	hypomorphic
Q171A	32-fold loss, ORN 79-fold loss, CP	lowest thermal stability with CP	–	trimer	N/A
D263A	N/A	++	+++	trimer	amorphic
D263N	1.4×10^5-fold loss, ORN 3.0×10^2-fold loss, CP	++	+++	trimer	hypomorphic
H302L	58-fold loss, ORN 78-fold loss, CP	++	470-fold	trimer	amorphic
C303A	25-fold loss, ORN 2-fold loss, CP	+++	+++	trimer	N/A
K307A	120-fold loss, ORN 0.87-fold loss, CP	+++	12-fold	trimer	N/A
K307E	54-fold loss, ORN 3.1-fold loss, CP	+++	–	trimer	hypomorphic
E310Q	17-fold loss, ORN 4.8-fold loss, CP	++	++	trimer	hypomorphic

[a]A change of ≤2 °C under any condition (+++) or a change of 3−6 °C (++). [b]No change or changes of <5-fold relative to that of the WT are indicated with three pluses. Changes between 5- and 10-fold relative to that of WT are indicated with two pluses. Changes of >10-fold are indicated with the fold decrease. [c]Growth deficiencies observed from hOTC expressed in yeast Δ*arg3* in ref 51. Amophic confers <5% growth of WT OTC. Hypomorphic confers 5−90% growth. Unimpaired is >90% growth of WT OTC.

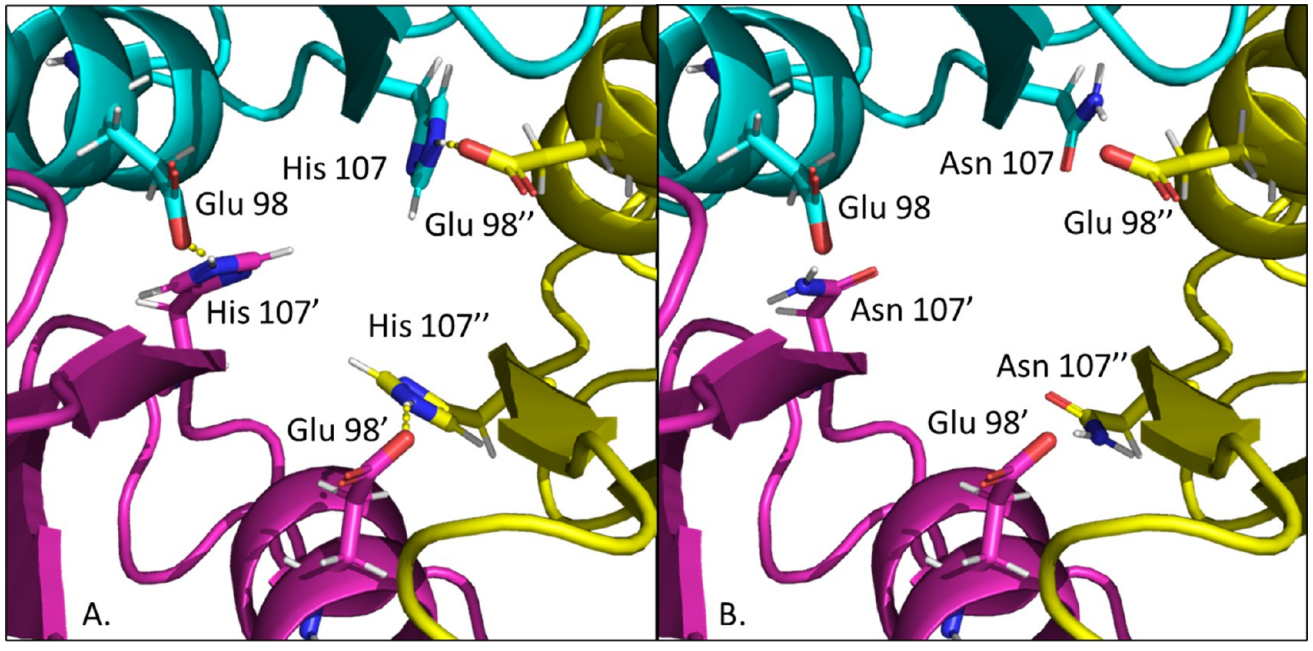

Figure 10. (A) Trimer center of WT hOTC showing interactions that are present between E98 and H107 in the subunits of the protein. (B) Trimer core of variant H107N, where the interactions between N107 and E98 in the subunits of the protein are weakened. Each subunit is shown in a different color (cyan, purple, and yellow). Prime and double-prime designations indicate the purple and yellow subunits, respectively.

H302Y had low activity in a human cell culture.[52] Even hOTC variants H302N and H302Q with relatively conservative mutations confererred hindered growth,[51] and hOTC H302N had ∼40% of the activity of WT hOTC in a human cell culture model.[51,52]

In this work, we identified two additional second-layer residues that are important for hOTC activity, namely, K307 and E310. hOTC variant K307E showed a 54-fold decrease in catalytic efficiency with respect to ORN and 3.1-fold decrease with respect to CP, but it still shows an increase in T_m in the presence of CP (Figure 3). Residue K307 is close to the SMG loop (∼3 Å) and is just outside the first-shell radius of the negatively charged carboxyl group of ORN (Figure 9D). A

https://doi.org/10.1021/acs.biochem.4c00206
Biochemistry 2024, 63, 1858−1875

charge repulsion might occur in the context of hOTC K307E, decreasing the rate of catalysis.

The removal of the charge in the hOTC K307A variant results in an increase in T_m in the presence of CP and phosphate relative to apo hOTC, but a 120-fold decrease in catalytic efficiency with respect to ORN. The kinetic results suggest that the loss of charge in this SMG-neighboring residue reduces the level of stabilization of the negatively charged carboxylate group of ORN and interferes with the hydrogen bond network that orients the ORN amine group. K307 is near L304, which is in the 302−305 ORN binding motif. The loss of the interaction between K307 and L304 could affect the orientation of ORN with respect to D263, reducing catalytic efficiency.

hOTC E310 was studied on the basis of its POOL rank, proximity to ORN, and previous work characterizing the corresponding residue E299 in *E. coli* OTC.[23] The thermal shift assay showed that the T_m of hOTC E310Q is lower than that of WT hOTC under all conditions. E310 is a second-shell residue that is 8 Å from ORN. Similar to K307, E310 is ∼4 Å from the SMG loop and the E310Q variant shows a significant decrease in catalytic efficiency with respect to ORN (17-fold decrease) and a smaller 4.8-fold decrease with respect to CP. In yeast complementation experiments, hOTC E301Q had a hypomorphic phenotype and intermediate growth,[51] whereas in human cell culture, hOTC E310G had ∼10% of the activity of WT hOTC and ∼50% of the steady state protein level as WT hOTC.[52] E310 has strong Coulombic coupling to D263 (1.2 kcal/mol), and the close match of the intrinsic pK_as (3.5 for D263 and 4.0 for E310) helps to expand the buffer range of D263, contributing to its catalytic potency (Table S2).[20] E310 forms a hydrogen bond with K307, and a mutation at this site could decrease the stability of the SMG loop and affect ORN binding (Figure 9D). The hOTC active site is located on flexible loops held together by an intricate hydrogen bonding network. Removal of important polar groups from these loops could affect substrate affinity and protein function.

POOL Predicts a Remote Fourth-Layer Residue That Is Important for hOTC Function. The mutation in the fourth layer H107N results in the second least stable variant reported here, although it still shows a substantial increase in T_m in the presence of CP. hOTC H107N exhibited a 4.7-fold decrease in catalytic efficiency with respect to ORN, a 66-fold decrease with respect to CP, and a 107-fold decrease in affinity for CP with respect to WT hOTC, consistent with the proximity of H107 to the CP binding residues. Although H107 is a fourth-layer residue, it is located at the trimer core and presumably has a role in stabilizing the hOTC trimer. Indeed, hOTC H107N showed the smallest R_g of any variant and has an altered SEC elution profile. It is possible that the hydrogen bond formed between H107 and E98 (Figure 10A) in adjacent subunits is an essential interaction that keeps the quaternary structure intact. When H107 is mutated to N107, these native Coulombic interactions are no longer present (Figure 10B) and the trimer core is destabilized. To test this hypothesis, we mutated E98 to Q, removing the charged interaction. The SEC profile of hOTC E98Q shows a mixture of the monomer, dimer, and trimer (Figure 8), implying that it destabilizes the core but to a lesser extent than the H107N mutation. In a yeast complementation experiment, hOTC mutation E98Q conferred hindered growth but not as extreme as that of mutations E98K and E98V, which caused <5% growth compared to that of WT hOTC. Human OTC E98K has shown very low enzymatic activity and greatly reduced protein levels in human cell culture.[52] Interestingly, none of the mutations of H107 caused the amorphic phenotype[51] and H107N conferred only slightly decreased growth.[51]

hOTC variant A152V was chosen as a negative control due to the low POOL rank and high conservation score of A152 from ConSurf. Kinetic studies with hOTC variant A152V demonstrated that this residue does not play a significant role in the enzymatic activity. The clinical manifestations of disease associated with variant A152V most likely do not arise from impaired catalytic activity but could be due to reduced stability (Figure 3). In yeast complemented with hOTC, variant A152V conferred a decreased level of growth, consistent with the phenotype seen in clinical manifestations.[51]

CONCLUSIONS

We have demonstrated the importance of D263 for hOTC catalytic function, with mutations at this site rendering the protein substantially less efficient, whereas C303 plays a role but is less important for activity (Table 6). We have newly identified three distal residues that are important for catalysis, H107, K307, and E310, that are 15, 6, and 8 Å, respectively, from the substrates and not previously known to be important for hOTC activity. We have confirmed the importance of a fourth distal residues, H302, previously identified as likely important for catalysis.[5] hOTC variants K307A, K307E, and E310Q are shown here to have reduced activity, especially with respect to ORN. The distal K307 and E310 are adjacent to the SMG loop and offer stability to the flexible region, allowing for the orientation of ORN needed for catalysis. Mutation of fourth-shell residue H107 results in reduced activity with respect to CP and is important for maintaining the quaternary structure. hOTC E98Q has the lowest T_m of all variants studied and is important for maintaining the quaternary structure. Second-shell residue H302 is part of the motif believed to stabilize the CP-ORN tetrahedral intermediate, and the OTCD-associated hOTC H302L variant caused a significant loss of catalytic efficiency with respect to both ORN and CP. The observations reported herein suggest the importance of not just first-shell residues but POOL-predicted distal residues that do not have direct contact with either substrate molecule. Understanding the role of proximal and distal residues in the activity of hOTC will help to elucidate the impact of OTCD-associated mutations on the catalytic function of hOTC.

ASSOCIATED CONTENT

Data Availability Statement

All data are contained in the manuscript or its Supporting Information.

Supporting Information

The Supporting Information is available free of charge at https://pubs.acs.org/doi/10.1021/acs.biochem.4c00206.

Sequence and structure alignments, Michaelis−Menten curves, coupling data, binding curves, semilog and Kratky plots, and size exclusion chromatograms (PDF)

Accession Codes

UniProt entry P00480.

https://doi.org/10.1021/acs.biochem.4c00206
Biochemistry 2024, 63, 1858−1875

AUTHOR INFORMATION

Corresponding Authors

Penny J. Beuning − *Department of Chemistry and Chemical Biology and Department of Bioengineering, Northeastern University, Boston, Massachusetts 02115, United States;* orcid.org/0000-0002-7770-022X; Email: beuning@neu.edu

Mary Jo Ondrechen − *Department of Chemistry and Chemical Biology and Department of Bioengineering, Northeastern University, Boston, Massachusetts 02115, United States;* orcid.org/0000-0003-2456-4313; Email: mjo@neu.edu

Authors

Samantha S. Watson − *Department of Chemistry and Chemical Biology, Northeastern University, Boston, Massachusetts 02115, United States*

Emily Micheloni − *Department of Chemistry and Chemical Biology, Northeastern University, Boston, Massachusetts 02115, United States*

Lisa Ngu − *Department of Chemistry and Chemical Biology, Northeastern University, Boston, Massachusetts 02115, United States*

Kelly K. Barnsley − *Department of Chemistry and Chemical Biology, Northeastern University, Boston, Massachusetts 02115, United States*

Lee Makowski − *Department of Chemistry and Chemical Biology and Department of Bioengineering, Northeastern University, Boston, Massachusetts 02115, United States;* orcid.org/0000-0003-0202-9264

Complete contact information is available at: https://pubs.acs.org/10.1021/acs.biochem.4c00206

Author Contributions

S.S.W. and E.M. contributed equally to this work. S.S.W.: conceptualization, methodology, software, and preparation of the original draft. E.M.: conceptualization, methodology, software, and reviewing and editing. L.N.: conceptualization, methodology, and software. K.K.B.: conceptualization, computation, and reviewing. L.M.: supervision, conceptualization, and reviewing and editing. P.J.B.: supervision, conceptualization, and reviewing and editing. M.J.O.: supervision, conceptualization, computation, and reviewing and editing.

Funding

This work was supported by National Science Foundation (NSF) Grants MCB-1517290 and MCB-2147498 to M.J.O. and P.J.B. The Nanotemper Monolith was obtained under National Institutes of Health (NIH) Grant 1S10OD030369-01 and is managed by the CILS facility at Northeastern University. The work is based in part on research conducted at the Center for High-Energy X-ray Sciences (CHEXS), which is supported by the NSF (BIO, ENG, and MPS Directorates) under Grant DMR-1829070., and the Macromolecular Diffraction at CHESS (MacCHESS) facility, which is supported by Grant 1-P30-GM124166-01A1 from the National Institute of General Medical Sciences (NIGMS), National Institutes of Health and by New York State's Empire State Development Corporation (NYSTAR). The LiX beamline is part of the Center for BioMolecular Structure (CBMS), which was primarily supported by the NIGMS through a P30 grant (Grant P30GM133893), and by the U.S. Department of Energy (DOE) Office of Biological and Environmental Research (Grant KP1605010). LiX also received additional support from the NIH (Grant S10 OD012331). As part of NSLS-II, a national user facility at Brookhaven National Laboratory, work performed at the CBMS was supported in part by the DOE, Office of Science, Office of Basic Energy Sciences (Contract DE-SC0012704).

Notes

The authors declare no competing financial interest.

ACKNOWLEDGMENTS

The authors gratefully acknowledge Prof. George O'Doherty (Northeastern University) for the use of his plate reader, Dr. Dashuang Shi (Children's National Medical Center) for the expression plasmid for hOTC, Lin Yang (LiX), Richard Gillilan, and Qingqiu Huang (CHESS) for assistance, and Michael Bergman (Deravi Lab, Northeastern University) for the use of their SEC column.

REFERENCES

(1) Brusilow, S. W. In *Urea Cycle Enzyme*; Valle, D. L., Antonarakis, S., Ballabio, A., Beaudet, A. L., Mitchell, G. A., Eds.; McGraw-Hill, 2019.

(2) Brusilow, S. W.; Maestri, N. E. Urea cycle disorders: diagnosis, pathophysiology, and therapy. *Adv. Pediatr* **1996**, *43*, 127−170.

(3) Dionisi-Vici, C.; Rizzo, C.; Burlina, A. B.; Caruso, U.; Sabetta, G.; Uziel, G.; Abeni, D. Inborn errors of metabolism in the Italian pediatric population: a national retrospective survey. *J. Pediatr* **2002**, *140* (3), 321−327.

(4) Keskinen, P.; Siitonen, A.; Salo, M. Hereditary urea cycle diseases in Finland. *Acta Paediatr* **2008**, *97* (10), 1412−1419.

(5) Shi, D.; Morizono, H.; Yu, X.; Tong, L.; Allewell, N. M.; Tuchman, M. Human ornithine transcarbamylase: crystallographic insights into substrate recognition and conformational changes. *Biochem. J.* **2001**, *354* (3), 501−509.

(6) Tuchman, M.; Morizono, H.; Reish, O.; Yuan, X.; Allewell, N. M. The molecular basis of ornithine transcarbamylase deficiency: modelling the human enzyme and the effects of mutations. *J. Med. Genet* **1995**, *32* (9), 680−688.

(7) Caldovic, L.; Abdikarim, I.; Narain, S.; Tuchman, M.; Morizono, H. Genotype-Phenotype Correlations in Ornithine Transcarbamylase Deficiency: A Mutation Update. *J. Genet Genomics* **2015**, *42* (5), 181−194.

(8) Stebbins, J. W.; Xu, W.; Kantrowitz, E. R. Three residues involved in binding and catalysis in the carbamyl phosphate binding site of *Escherichia coli* aspartate transcarbamylase. *Biochemistry* **1989**, *28* (6), 2592−2600.

(9) Shi, D.; Morizono, H.; Aoyagi, M.; Tuchman, M.; Allewell, N. M. Crystal structure of human ornithine transcarbamylase complexed with carbamoyl phosphate and L-norvaline at 1.9 A resolution. *Proteins* **2000**, *39* (4), 271−277.

(10) Shi, D.; Morizono, H.; Ha, Y.; Aoyagi, M.; Tuchman, M.; Allewell, N. M. 1.85-A resolution crystal structure of human ornithine transcarbamoylase complexed with N-phosphonacetyl-L-ornithine. Catalytic mechanism and correlation with inherited deficiency. *J. Biol. Chem.* **1998**, *273* (51), 34247−34254.

(11) Ke, H. M.; Lipscomb, W. N.; Cho, Y. J.; Honzatko, R. B. Complex of N-phosphonacetyl-L-aspartate with aspartate carbamoyltransferase. X-ray refinement, analysis of conformational changes and catalytic and allosteric mechanisms. *J. Mol. Biol.* **1988**, *204* (3), 725−747.

(12) Tuchman, M.; Jaleel, N.; Morizono, H.; Sheehy, L.; Lynch, M. G. Mutations and polymorphisms in the human ornithine transcarbamylase gene. *Hum Mutat* **2002**, *19* (2), 93−107.

(13) McDowall, S.; van Heeswijck, R.; Hoogenraad, N. Site-directed mutagenesis of Arg60 and Cys271 in ornithine transcarbamylase from rat liver. *Protein Eng.* **1990**, *4* (1), 73−77.

(14) Goldsmith, J. O.; Lee, S.; Zambidis, I.; Kuo, L. C. Control of L-ornithine specificity in *Escherichia coli* ornithine transcarbamoylase. Site-directed mutagenic and pH studies. *J. Biol. Chem.* **1991**, *266* (28), 18626−18634.
(15) Tong, W.; Wei, Y.; Murga, L. F.; Ondrechen, M. J.; Williams, R. J. Partial order optimum likelihood (POOL): maximum likelihood prediction of protein active site residues using 3D Structure and sequence properties. *PLoS Comput. Biol.* **2009**, *5* (1), No. e1000266.
(16) Somarowthu, S.; Yang, H.; Hildebrand, D. G.; Ondrechen, M. J. High-performance prediction of functional residues in proteins with machine learning and computed input features. *Biopolymers* **2011**, *95* (6), 390−400.
(17) Ondrechen, M. J.; Clifton, J. G.; Ringe, D. THEMATICS: a simple computational predictor of enzyme function from structure. *Proc. Natl. Acad. Sci. U. S. A.* **2001**, *98* (22), 12473−12478.
(18) Ringe, D.; Wei, Y.; Boino, K. R.; Ondrechen, M. J. Protein Structure to Function: Insights from Computation. *Cell. Mol. Life Sci.* **2004**, *61*, 387−392.
(19) Capra, J. A.; Laskowski, R. A.; Thornton, J. M.; Singh, M.; Funkhouser, T. A. Predicting protein ligand binding sites by combining evolutionary sequence conservation and 3D structure. *PLoS Comput. Biol.* **2009**, *5* (12), No. e1000585.
(20) Coulther, T. A.; Ko, J.; Ondrechen, M. J. Amino acid interactions that facilitate enzyme catalysis. *J. Chem. Phys.* **2021**, *154* (19), 195101 DOI: 10.1063/5.0041156.
(21) Somarowthu, S.; Brodkin, H. R.; D'Aquino, J. A.; Ringe, D.; Ondrechen, M. J.; Beuning, P. J. A tale of two isomerases: compact versus extended active sites in ketosteroid isomerase and phosphoglucose isomerase. *Biochemistry* **2011**, *50* (43), 9283−9295.
(22) Brodkin, H. R.; Novak, W. R. P.; Milne, A. C.; D'Aquino, J. A.; Karabacak, N. M.; Goldberg, I. G.; Agar, J. N.; Payne, M. S.; Petsko, G. A.; Ondrechen, M. J.; et al. Evidence of the participation of remote residues in the catalytic activity of Co-type nitrile hydratase from *Pseudomonas putida*. *Biochemistry* **2011**, *50* (22), 4923−4935.
(23) Ngu, L.; Winters, J. N.; Nguyen, K.; Ramos, K. E.; DeLateur, N. A.; Makowski, L.; Whitford, P. C.; Ondrechen, M. J.; Beuning, P. J. Probing remote residues important for catalysis in *Escherichia coli* ornithine transcarbamoylase. *PLoS One* **2020**, *15* (2), No. e0228487.
(24) Brodkin, H. R.; DeLateur, N. A.; Somarowthu, S.; Mills, C. L.; Novak, W. R.; Beuning, P. J.; Ringe, D.; Ondrechen, M. J. Prediction of distal residue participation in enzyme catalysis. *Protein Sci.* **2015**, *24* (5), 762−778.
(25) Parasuram, R.; Coulther, T. A.; Hollander, J. M.; Keston-Smith, E.; Ondrechen, M. J.; Beuning, P. J. Prediction of Active Site and Distal Residues in *E. coli* DNA Polymerase III alpha Polymerase Activity. *Biochemistry* **2018**, *57* (7), 1063−1072.
(26) Walsh, J. M.; Parasuram, R.; Rajput, P. R.; Rozners, E.; Ondrechen, M. J.; Beuning, P. J. Effects of non-catalytic, distal amino acid residues on activity of *E. coli* DinB (DNA polymerase IV). *Environ. Mol. Mutagen* **2012**, *53* (9), 766−776.
(27) Kuo, L. C.; Herzberg, W.; Lipscomb, W. N. Substrate specificity and protonation state of ornithine transcarbamoylase as determined by pH studies. *Biochemistry* **1985**, *24* (18), 4754−4761.
(28) Krieger, E.; Vriend, G. YASARA View - molecular graphics for all devices - from smartphones to workstations. *Bioinformatics* **2014**, *30* (20), 2981−2982.
(29) Iyengar, S. M.; Barnsley, K. K.; Xu, R.; Prystupa, A.; Ondrechen, M. J. Electrostatic fingerprints of catalytically active amino acids in enzymes. *Protein Sci.* **2022**, *31* (5), No. e4291.
(30) Morizono, H.; Tuchman, M.; Rajagopal, B. S.; McCann, M. T.; Listrom, C. D.; Yuan, X.; Venugopal, D.; Barany, G.; Allewell, N. M. Expression, purification and kinetic characterization of wild-type human ornithine transcarbamylase and a recurrent mutant that produces 'late onset' hyperammonaemia. *Biochem. J.* **1997**, *322* (2), 625−631.
(31) Pastra-Landis, S. C.; Foote, J.; Kantrowitz, E. R. An improved colorimetric assay for aspartate and ornithine transcarbamylases. *Anal. Biochem.* **1981**, *118* (2), 358−363.
(32) Boyde, T. R.; Rahmatullah, M. Optimization of conditions for the colorimetric determination of citrulline, using diacetyl monoxime. *Anal. Biochem.* **1980**, *107* (2), 424−431.
(33) Ericsson, U. B.; Hallberg, B. M.; Detitta, G. T.; Dekker, N.; Nordlund, P. Thermofluor-based high-throughput stability optimization of proteins for structural studies. *Anal. Biochem.* **2006**, *357* (2), 289−298.
(34) Acerbo, A. S.; Cook, M. J.; Gillilan, R. E. Upgrade of MacCHESS facility for X-ray scattering of biological macromolecules in solution. *J. Synchrotron Radiat* **2015**, *22* (1), 180−186.
(35) Skou, S.; Gillilan, R. E.; Ando, N. Synchrotron-based small-angle X-ray scattering of proteins in solution. *Nat. Protoc* **2014**, *9* (7), 1727−1739.
(36) Hopkins, J. B.; Gillilan, R. E.; Skou, S. BioXTAS RAW: improvements to a free open-source program for small-angle X-ray scattering data reduction and analysis. *J. Appl. Crystallogr.* **2017**, *50* (5), 1545−1553.
(37) Svergun, D. I. Determination of the regularization parameter in indirect-transform methods using perceptual criteria. *J. Appl. Crystallogr.* **1992**, *25* (4), 495−503.
(38) Svergun, D. I.; Petoukhov, M. V.; Koch, M. H. Determination of domain structure of proteins from X-ray solution scattering. *Biophys. J.* **2001**, *80* (6), 2946−2953.
(39) Pettersen, E. F.; Goddard, T. D.; Huang, C. C.; Couch, G. S.; Greenblatt, D. M.; Meng, E. C.; Ferrin, T. E. UCSF Chimera–a visualization system for exploratory research and analysis. *J. Comput. Chem.* **2004**, *25* (13), 1605−1612.
(40) Franke, D.; Petoukhov, M. V.; Konarev, P. V.; Panjkovich, A.; Tuukkanen, A.; Mertens, H. D. T.; Kikhney, A. G.; Hajizadeh, N. R.; Franklin, J. M.; Jeffries, C. M.; Svergun, D. I.; et al. ATSAS 2.8: a comprehensive data analysis suite for small-angle scattering from macromolecular solutions. *J. Appl. Crystallogr.* **2017**, *50* (4), 1212−1225.
(41) Ashkenazy, H.; Abadi, S.; Martz, E.; Chay, O.; Mayrose, I.; Pupko, T.; Ben-Tal, N. ConSurf 2016: an improved methodology to estimate and visualize evolutionary conservation in macromolecules. *Nucleic Acids Res.* **2016**, *44* (W1), W344−W350.
(42) Tuchman, M.; Morizono, H.; Rajagopal, B. S.; Plante, R. J.; Allewell, N. M. Identification of 'private' mutations in patients with ornithine transcarbamylase deficiency. *J. Inherit Metab Dis* **1997**, *20* (4), 525−527.
(43) Tuchman, M.; Morizono, H.; Rajagopal, B. S.; Plante, R. J.; Allewell, N. M. The biochemical and molecular spectrum of ornithine transcarbamylase deficiency. *J. Inherited Metab. Dis.* **1998**, *21* (S1), 40−58.
(44) Kuo, L. C.; Caron, C.; Lee, S.; Herzberg, W. Zn^{2+} regulation of ornithine transcarbamoylase. II. Metal binding site. *J. Mol. Biol.* **1990**, *211* (1), 271−280.
(45) Marshall, M.; Cohen, P. P. The essential sulfhydryl group of ornithine transcarbamylases. Reaction with anionic, aromatic disulfides and properties of its cyano derivative. *J. Biol. Chem.* **1980**, *255* (15), 7291−7295.
(46) Sankaranarayanan, R.; Cherney, M. M.; Cherney, L. T.; Garen, C. R.; Moradian, F.; James, M. N. The crystal structures of ornithine carbamoyltransferase from *Mycobacterium tuberculosis* and its ternary complex with carbamoyl phosphate and L-norvaline reveal the enzyme's catalytic mechanism. *J. Mol. Biol.* **2008**, *375* (4), 1052−1063.
(47) Knight, C. J.; Hub, J. S. WAXSiS: a web server for the calculation of SAXS/WAXS curves based on explicit-solvent molecular dynamics. *Nucleic Acids Res.* **2015**, *43* (W1), W225−W230.
(48) De Gregorio, A.; Risitano, A.; Capo, C.; Crinio, C.; Petruzzelli, R.; Desideri, A. Evidence of carbamoylphosphate induced conformational changes upon binding to human ornithine carbamoyltransferase. *Biochem Mol. Biol. Int.* **1999**, *47* (6), 965−970.
(49) Miller, A. W.; Kuo, L. C. Ligand-induced isomerizations of *Escherichia coli* ornithine transcarbamoylase. An ultraviolet difference analysis. *J. Biol. Chem.* **1990**, *265* (25), 15023−15027.

(50) Fleming, P. J.; Fleming, K. G. HullRad: Fast Calculations of Folded and Disordered Protein and Nucleic Acid Hydrodynamic Properties. *Biophys. J.* **2018**, *114* (4), 856−869.
(51) Lo, R. S.; Cromie, G. A.; Tang, M.; Teng, K.; Owens, K.; Sirr, A.; Kutz, J. N.; Morizono, H.; Caldovic, L.; Ah Mew, N.; et al. The functional impact of 1,570 individual amino acid substitutions in human OTC. *Am. J. Hum. Genet.* **2023**, *110* (5), 863−879.
(52) Scharre, S.; Posset, R.; Garbade, S. F.; Gleich, F.; Seidl, M. J.; Druck, A. C.; Okun, J. G.; Gropman, A. L.; Nagamani, S. C. S.; Hoffmann, G. F.; et al. Predicting the disease severity in male individuals with ornithine transcarbamylase deficiency. *Ann. Clin Transl Neurol* **2022**, *9* (11), 1715−1726.
(53) Akhmedov, D.; Braun, M.; Mataki, C.; Park, K. S.; Pozzan, T.; Schoonjans, K.; Rorsman, P.; Wollheim, C. B.; Wiederkehr, A. Mitochondrial matrix pH controls oxidative phosphorylation and metabolism-secretion coupling in INS-1E clonal beta cells. *FASEB J.* **2010**, *24* (11), 4613−4626.
(54) Robey, E. A.; Wente, S. R.; Markby, D. W.; Flint, A.; Yang, Y. R.; Schachman, H. K. Effect of amino acid substitutions on the catalytic and regulatory properties of aspartate transcarbamoylase. *Proc. Natl. Acad. Sci. U. S. A.* **1986**, *83* (16), 5934−5938.

https://doi.org/10.1021/acs.biochem.4c00206
Biochemistry 2024, 63, 1858−1875